



Calhoun: The NPS Institutional Archive
DSpace Repository

Theses and Dissertations

1. Thesis and Dissertation Collection, all items

2008-03

Investigation of the transmission of sound
through isotropic, damped material layer(s)
bounded by seawater

Roche, Gerald J.

Monterey California. Naval Postgraduate School

Downloaded from NPS Archive: Calhoun



<http://www.nps.edu/library>

Calhoun is the Naval Postgraduate School's public access digital repository for research materials and institutional publications created by the NPS community. Calhoun is named for Professor of Mathematics Guy K. Calhoun, NPS's first appointed -- and published -- scholarly author.

Dudley Knox Library / Naval Postgraduate School
411 Dyer Road / 1 University Circle
Monterey, California USA 93943



NAVAL POSTGRADUATE SCHOOL

MONTEREY, CALIFORNIA

THESIS

**INVESTIGATION OF THE TRANSMISSION OF SOUND
THROUGH ISOTROPIC, DAMPED MATERIAL LAYER(S)
BOUNDED BY SEAWATER**

by

Gerald J. Roche

March 2008

Thesis Advisor:
Second Reader:

Clyde Scandrett
Thomas Ramotowski

Approved for public release, distribution is unlimited

THIS PAGE INTENTIONALLY LEFT BLANK

REPORT DOCUMENTATION PAGE			<i>Form Approved OMB No. 0704-0188</i>	
Public reporting burden for this collection of information is estimated to average 1 hour per response, including the time for reviewing instruction, searching existing data sources, gathering and maintaining the data needed, and completing and reviewing the collection of information. Send comments regarding this burden estimate or any other aspect of this collection of information, including suggestions for reducing this burden, to Washington headquarters Services, Directorate for Information Operations and Reports, 1215 Jefferson Davis Highway, Suite 1204, Arlington, VA 22202-4302, and to the Office of Management and Budget, Paperwork Reduction Project (0704-0188) Washington DC 20503.				
1. AGENCY USE ONLY (Leave blank)		2. REPORT DATE March 2008	3. REPORT TYPE AND DATES COVERED Master's Thesis	
4. TITLE AND SUBTITLE Investigation of the Transmission of Sound Through Isotropic, Damped Material Layer(s) Bounded by Seawater			5. FUNDING NUMBERS	
6. AUTHOR(S) : Roche, Gerald J.				
7. PERFORMING ORGANIZATION NAME(S) AND ADDRESS(ES) Naval Postgraduate School Monterey, CA 93943-5000			8. PERFORMING ORGANIZATION REPORT NUMBER	
9. SPONSORING /MONITORING AGENCY NAME(S) AND ADDRESS(ES) N/A			10. SPONSORING/MONITORING AGENCY REPORT NUMBER	
11. SUPPLEMENTARY NOTES The views expressed in this thesis are those of the author and do not reflect the official policy or position of the Department of Defense or the U.S. Government.				
12a. DISTRIBUTION / AVAILABILITY STATEMENT Approved for public release, distribution is unlimited			12b. DISTRIBUTION CODE	
13. ABSTRACT (maximum 200 words) Acoustic 'windows' are used in SONAR applications to absorb structural loads associated with the platform operation while allowing the passage of acoustic signals. The performance metric commonly used to gauge the acoustic window quality is insertion loss. This thesis provides a derivation of insertion loss for multi-layered materials as a function of frequency and angle of incidence. Derivations are modified to include attenuation of the signals in the material and the result has been written into a MATLAB model. Measurements on single layer plastic, polyurethane and steel panels show good experimental agreement with the theoretical model. The model is then used to predict insertion loss of multiple layers as a tool for improving window bending rigidity.				
14. SUBJECT TERMS Insertion Loss, Acoustic Materials, Transmission Loss			15. NUMBER OF PAGES 69	
			16. PRICE CODE	
17. SECURITY CLASSIFICATION OF REPORT Unclassified	18. SECURITY CLASSIFICATION OF THIS PAGE Unclassified	19. SECURITY CLASSIFICATION OF ABSTRACT Unclassified	20. LIMITATION OF ABSTRACT UU	

NSN 7540-01-280-5500

Standard Form 298 (Rev. 2-89)
Prescribed by ANSI Std. Z39-18

THIS PAGE INTENTIONALLY LEFT BLANK

Approved for public release, distribution is unlimited

**INVESTIGATION OF THE TRANSMISSION OF SOUND THROUGH
ISOTROPIC, DAMPED MATERIAL LAYER(S) BOUNDED BY SEAWATER**

Gerald J. Roche
Engineer, Naval Undersea Warfare Center, Division Newport
B.S.M.E., Southern Illinois University, 1998

Submitted in partial fulfillment of the
requirements for the degree of

MASTER OF SCIENCE IN ENGINEERING ACOUSTICS

from the

**NAVAL POSTGRADUATE SCHOOL
March 2008**

Author: Gerald J. Roche

Approved by: Dr. Clyde Scandrett
Thesis Advisor

Thomas Ramotowski
Second Reader

Dr. Kevin Smith
Chair, Engineering Acoustics Academic Committee

THIS PAGE INTENTIONALLY LEFT BLANK

ABSTRACT

Acoustic ‘windows’ are used in SONAR applications to absorb structural loads associated with the platform operation while allowing the passage of acoustic signals. The performance metric commonly used to gauge the acoustic window quality is insertion loss. This thesis provides a derivation of insertion loss for multi-layered materials as a function of frequency and angle of incidence. Derivations are modified to include attenuation of the signals in the material and the result has been written into a MATLAB model. Measurements on single layer plastic, polyurethane and steel panels show good experimental agreement with the theoretical model. The model is then used to predict insertion loss of multiple layers as a tool for improving window bending rigidity.

THIS PAGE INTENTIONALLY LEFT BLANK

TABLE OF CONTENTS

I.	INTRODUCTION.....	1
A.	ACOUSTIC WINDOWS.....	1
1.	Operational Loads	1
2.	Acoustic Performance.....	2
B.	TYPICAL MATERIALS	5
C.	PREVIOUS WORK.....	6
II.	THEORY	9
A.	SINGLE LAYER NORMAL INCIDENCE	9
B.	MULTI-LAYER NON-NORMAL INCIDENCE	10
1.	Stress/Strain Wave Propagation.....	10
2.	Non-Normal, Multi-Layered, Unattenuated Case	14
3.	Non-Normal, Multi-Layer, Attenuated Case.....	18
III.	MEASUREMENTS AND MODELS	25
A.	MEASUREMENTS	25
B.	MODEL	28
C.	NORMAL INCIDENCE MODELS AND MEASUREMENTS	29
D.	NON-NORMAL INCIDENCE MODELS AND MEASUREMENTS	34
IV.	COMMENTS AND DISCUSSION	37
A.	DESIGN IMPROVEMENT	37
B.	FUTURE WORK	44
	APPENDIX. MATLAB CODE	45
	LIST OF REFERENCES	51
	INITIAL DISTRIBUTION LIST	53

THIS PAGE INTENTIONALLY LEFT BLANK

LIST OF FIGURES

Figure 1.	Intensity transmission coefficient for steel plate (1 cm thick) at 250kHz. Angles are measured from normal to the interface.	3
Figure 2.	Directivity function for a line array for $s=10$ positioned behind a steel plate (1 cm thick) at 250kHz.	4
Figure 3.	Insertion loss v transmission loss.	10
Figure 4.	Traction vectors acting on orthogonal planes of a differential element from [10].	11
Figure 5.	Traction vector components acting on a differential element from [10].	12
Figure 6.	Shear strain definition from [10].	12
Figure 7.	Wave propagation direction.	15
Figure 8.	Acoustic Measurement Setup	25
Figure 9.	Minimum panel to address edge diffraction.	27
Figure 10.	Minimum required panel length L_2 and maximum hydrophone length L_1	27
Figure 11.	Insertion loss of 1.905cm cast Nylon 6 panel at normal incidence.	30
Figure 12.	Insertion loss of 2.54cm Noryl EN-265 panel at normal incidence.	30
Figure 13.	Insertion loss of 1.0cm A36 carbon steel plate at normal incidence.	31
Figure 14.	Insertion loss of 1.0cm A36 carbon steel plate at normal incidence with measured data points fit with a 3 rd order polynomial curve.	32
Figure 15.	Insertion loss of 0.635cm thick PR-1574 panel at normal incidence.	33
Figure 16.	Insertion loss of 0.635 cm thick PR-1574 panel with low (0.015) loss tangent.	33
Figure 17.	Insertion loss of 1.905cm thick Cast Nylon 6 panel at 15° incidence.	34
Figure 18.	Insertion loss of 1.0cm thick A36 carbon steel panel at 20° incidence.	35
Figure 19.	Insertion loss of 0.635cm thick PR1574 panel at 30° incidence.	36
Figure 20.	Model 3 insertion loss prediction of ALUM-PR1574-ALUM 'sandwich' composite with properties as shown in Table 8.	39
Figure 21.	Contour plot of insertion loss (dB) prediction of ALUM-PR1574-ALUM 'sandwich' composite with properties as shown in Table 8.	40
Figure 22.	Contour plot of insertion loss (dB) prediction of ALUM-PR1574-ALUM 'sandwich' composite with properties as shown in Table 8, but with the Young's modulus of layers 1 & 3 changed to from 70 to 55GPa.	41
Figure 23.	Contour plot of insertion loss (dB) prediction of ALUM-PR1574-ALUM 'sandwich' composite with properties as shown in Table 8, but with the Young's modulus of layers 1 & 3 changed to from 70 to 7GPa.	42
Figure 24.	Contour plot of insertion loss (dB) prediction of STEEL-PR1574-STEEL 'sandwich' composite with properties as shown in Table 9.	43

THIS PAGE INTENTIONALLY LEFT BLANK

LIST OF TABLES

Table 1.	Characteristic impedance match of common structural materials to water	5
Table 2.	Mechanical properties of common structural materials.....	6
Table 3.	Thesis Bounds.....	6
Table 4.	The number of independent stiffness coefficients (n_{sc}) for various crystal types.	14
Table 5.	List of boundary conditions for general case of normal and non-normal incidence.	15
Table 6.	Physical properties for single layer, isotropic materials used in the test cases.	29
Table 7.	Bending rigidity for an ALUM-PR1574-ALUM composite section and a PR1574 constant section for a given thickness.....	38
Table 8.	Layered material 1:ALUM-PR1574-ALUM.	38
Table 9.	Layered material 2: Steel-PR1574-Steel.....	43

THIS PAGE INTENTIONALLY LEFT BLANK

ACKNOWLEDGMENTS

The author wishes to thank the following people for contributing to the thesis: Dr. Clyde Scandrett of Naval Postgraduate School for the many timely and helpful correspondence with the author, Tony Paolero of Naval Undersea Warfare Center (NUWC), Newport, RI, Underwater Sound Reference Division (USRD) for help in gathering acoustic measurement data, Tom Ramotowski, also of NUWC, for his many helpful discussions on acoustic windows over the years and for his comments as a second reader, and finally my wife, Robin, for the countless sacrifices made during the years leading up to this accomplishment.

THIS PAGE INTENTIONALLY LEFT BLANK

I. INTRODUCTION

A. ACOUSTIC WINDOWS

Acoustic ‘windows’ and ‘domes’ are used in Naval and commercial applications to protect associated underwater acoustic transducers and hydrophones from afloat debris and hydrodynamic loads, as well as to streamline the structure exposed to flow loads thereby reducing flow noise. Windows are mounted in the frame of the hull, typically positioned a few inches in front of the transducer/hydrophone which is in turn mounted in a flooded seachest. Tradeoffs must be made between required mechanical properties that support operational loads, and a need for optimal acoustic performance. These two requirements are typically mutually exclusive.

1. Operational Loads

Operational loads fall into two categories: structural and environmental.

Structural loads are typically considered in terms of normal pressures applied to the surface of the window. Such loads are caused by either hydrodynamic forces associated with the speed of the platform, or ‘wave slap’ applied to stationary platforms. Although stress in the material is a consideration, a larger concern is the displacement or strain of the window caused by bending under these loads. Significant changes in geometry caused by hydrodynamic loads, may degrade the streamlining of the window or dome shape which in turn could lead to unintended load and flow noise as well as cause damage to the window’s associated transducer. Displacements should therefore be minimized.

Environmental loads are in the form of external operating conditions such as temperature, hydrostatic pressure and long term seawater immersion. Windows must operate typically over a temperature range from 0-40°C, with structural stability required over the larger range of -40°C to 60°C. Many materials experience changes in critical material properties, such as strength, density, damping and elastic moduli, as functions of

temperature. Further changes are known to occur if water is absorbed by the material. Additionally, some materials experience significant dimensional (thickness) changes under hydrostatic load. Successful designs must consider and address all of these factors in optimizing the acoustic properties of windows employed.

2. Acoustic Performance

Acoustic performance of the window has a direct impact on the associated SONAR system performance. Ideally, acoustic signals scattered from a target should pass through the transducer window unchanged. In practice, signal strength varies as a function of the frequency and the incidence angle of the signal. Degradation of the former reduces the range at which targets can be identified by reducing the signal to noise ratio of the system, while uncertainty in the latter may cause ambiguity of target direction. These effects can be demonstrated by considering a simple line array.

Ziomek [1] derives the normalized far field directivity (D_N) function for a line array using the spatial Fourier transform of the complex aperture function, $A(f, x_a)$, defined as the complex signal produced by the array in response to a plane wave at the spatial location x_a and at the frequency f . For the case of spatial elements with identical response, $A(f, x_a)$ is defined as a “rectangular” (constant) amplitude window function, and the spatial Fourier transform produces a *sinc* directivity function, i.e.,

$D_N = \text{sinc} (s \sin \varphi)$ <p> $s = \text{array length/wavelength}$ $\varphi = \text{angle of incidence}$ $\text{measured from the normal}$ $\text{to the interface surface.}$ </p>
--

Equation 1. Line array directivity function

When an acoustic window is in the signal path, the aperture function used in the derivation of the directivity function should be modified as follows to account for the amplitude changes as a function of incidence angle:

$$A(f, x_a) \rightarrow A(f, x_a, \varphi) = \text{rect}(x_a/L) F(\varphi)$$

$$L = \text{length of aperture}$$

Equation 2. Modified aperture function

The resulting directivity function would then be the *sinc* function of Equation 1 scaled by $F(\varphi)$. The scaling function turns out to be equivalent to the square root of the intensity transmission coefficient (Γ) metric, defined as the ratio of acoustic intensity transmitted to the intensity that was incident [2]. Figure 1 and Figure 2 demonstrate the effect of scaling the *sinc* function by, in this case, the square root of the intensity transmission coefficient of a steel plate with an observed significant sidelobe level increase.

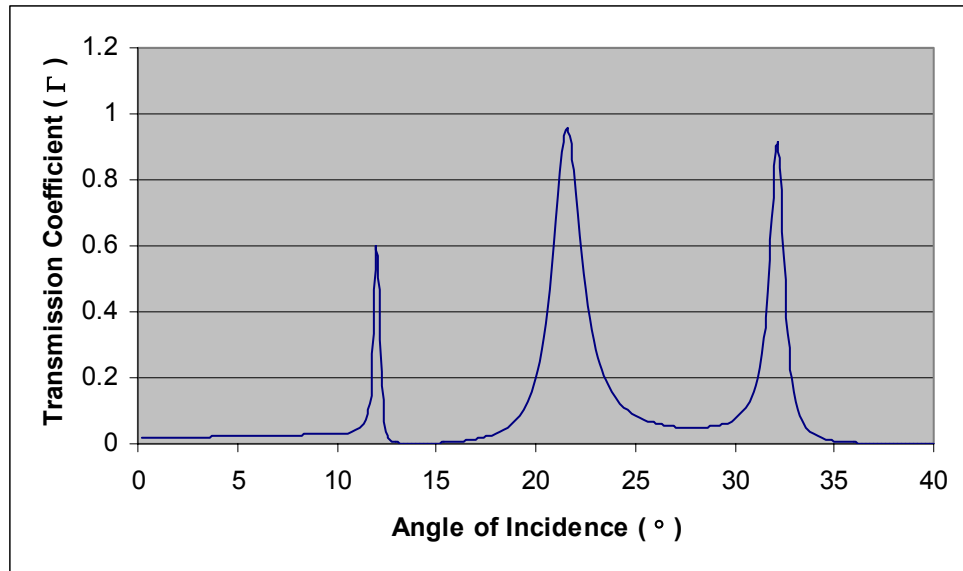


Figure 1. Intensity transmission coefficient for steel plate (1 cm thick) at 250kHz. Angles are measured from normal to the interface.

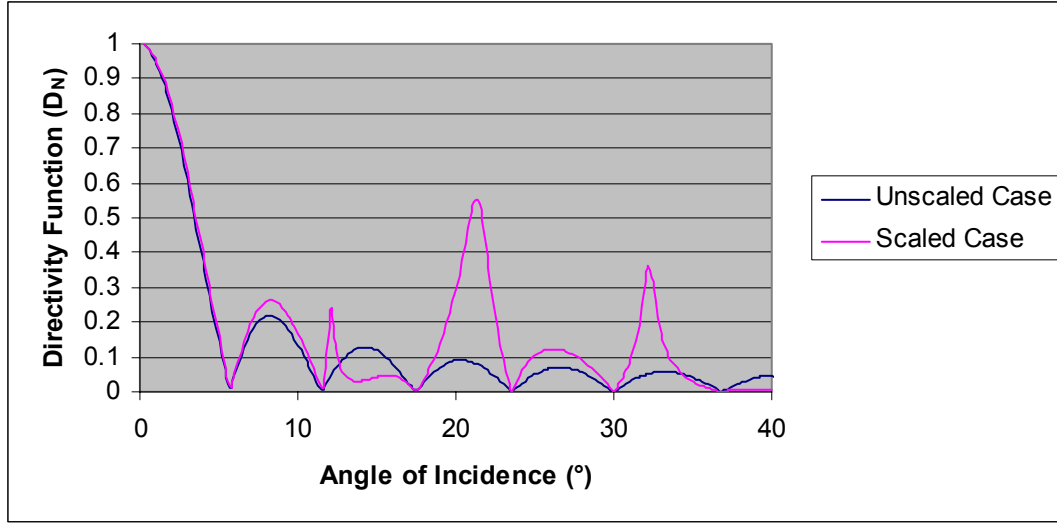


Figure 2. Directivity function for a line array for $s=10$ positioned behind a steel plate (1 cm thick) at 250kHz.

A widely used metric to gauge window performance is ‘insertion loss,’ defined as the logarithmic ratio of sound intensity at a fixed location with and without the window in the path of the sound wave [3].

$$\text{Insertion Loss} = 20 \log_{10} [P_1 / P_2] = 10 \log_{10} [1 / \Gamma]$$

P_1 = Pressure at fixed point without window in signal path

P_2 = Pressure at fixed point with window in signal path.

Equation 3. Typical insertion loss definition

Typical insertion loss levels on naval acoustic windows is 2dB or less. Using an electrical impedance analogy, a characteristic impedance, defined as the product of the material density (ρ) and the material sound speed (c), is commonly compared with the characteristic impedance of seawater as an indicator of window material performance. A second indicator is the ratio of material characteristic dimension to the wavelength. Ratios of characteristic dimensions of the window to wavelength that are much less than

one, produce near acoustic transparency. As such, in many ‘low’ frequency applications, materials with poor impedance match to water are still capable of overall satisfactory performance.

B. TYPICAL MATERIALS

Materials in common use for acoustic windows fall into the categories of rubber, polyurethane, fiber reinforced epoxy and engineering plastics. The first two groups, rubber and polyurethane, typically have good impedance (ρc) matches to water. Table 1 lists some common materials along and their associated ratio of characteristic impedance to that of water.

<i>Material</i>	<i>Density (ρ) g/cc</i>	<i>Longitudinal Sound Speed (c) m/s</i>	<i>(ρc)_{material} / (ρc)_{water}</i>
Rubber (Buna-n)	0.90	1550	1.0
Polyurethane (PR 1574)	1.01	1700	1.02
Plastic (Noryl EN-265)	1.08	2103	1.1
ALUM (6055)	2.7	6300	11
Steel (A36)	7.7	6100	30

Table 1. Characteristic impedance match of common structural materials to water

As stated above, there are frequency regimes and/or optimization methods available that allow the use of ‘poorly’ matched materials in cases where structural requirements exclude the use of materials with better impedance matches. Table 2 demonstrates the mutually exclusive nature of acoustic and mechanical/structural properties. Note that materials with good matches (ρc ratio ~ 1), per Table 1, also have relatively poor tensile strength and modulus values.

<i>Material</i>	<i>Tensile Strength (ksi)</i>	<i>Young's Modulus¹ (ksi)</i>
Rubber (Neoprene WRT)	1.5	0.4
Polyurethane (PR 1574)	2	0.8
Plastic (Noryl EN-265)	6	390
ALUM (6055)	40	10000
Steel (A36)	36	30000

Table 2. Mechanical properties of common structural materials

Windows with lateral dimensions approaching a wavelength have the added complication of exciting flexural waves in the window material. Bounds applied in this thesis, described below, will lessen these effects to the point that they may be neglected.

<i>Thesis Bound #</i>	<i>Condition</i>	<i>Condition</i>
1	panel thickness	< 2in.
2	frequency range	50-250kHz
3	angle of incidence	0-40°

Table 3. Thesis Bounds

C. PREVIOUS WORK

Research related to the general case of sound propagation through layered media is extensive. A detailed list of early work is reported in [4]. Specific examples include work by Fay [5] who presented a set of equations to predict transmission loss for a mono-layer plate, including comparisons of predicted and measured values for a steel plate demonstrating reasonable agreement. This simple modeling has been sufficient for many applications since mono-layer structures of rubber, polyurethane or plastic have been shown to satisfy acoustic and structural requirements in earlier window designs.

More recently, multi-layer designs have become necessary to meet strength and bending requirements unmet by mono-layer design windows. These multi-layered windows are considered composites and range from typical fiber reinforced epoxy ('fiberglass') to custom designs. Fiberglass designs have been acoustically characterized

¹ Quasi-static modulus listed.

empirically for specific applications and tend to be used for very low (<1) thickness/wavelength ratios because acoustic performance of these designs is otherwise poor. The nature of these low thickness/wavelength ratios requires lower frequency transducers that are typically larger, leading to larger dimensions of window aperture requiring in turn increased strength as load pressures need to be applied over a greater area. For higher thickness/wavelength ratio applications, customized windows such as those described in [6], where a modified epoxy resin is often used with a low density fiber ('Spectra') resulting in a window with macroscopic density and sound speed that is nearly ideal, have been used. Although these newer designs offer similar acoustic with improved structural performance relative to mono-layer designs, the ability to manufacture consistent quality customized composites has been poor. Recently Goodrich Corp. [7] has designed a multi-layered window, called RHO-COR®, that utilizes an elastomeric 'core' material bounded by layers of composite material and has been shown to satisfy acoustic and structural requirements for frequencies up to 50 kHz. A drawback is the fact that it is costly relative to mono-layer designs.

THIS PAGE INTENTIONALLY LEFT BLANK

II. THEORY

A. SINGLE LAYER NORMAL INCIDENCE

In the case of normal incidence sound waves passing from water through an isotropic, homogeneous solid, all points along the water-solid interface move in phase so no shear (transverse) wave is generated and the problem is significantly simplified.

As presented in [3], the intensity transmission coefficient (Γ) for a water bound homogeneous material is found to be:

$$\Gamma = | \mathbf{p}_{n,transmitted}^2 / \mathbf{p}_{n,incident}^2 | = 1 / [1 + .25([(\rho_2 c_2 / \rho_1 c_1) - (\rho_1 c_1 / \rho_2 c_2)]^2 \sin^2 k_2 L_t)]$$

where: $\omega = 2\pi f$, $c_1 = \text{speed of sound in water}$
 $c_2 = \text{speed of sound in material}$, $k_2 = \omega/c_2$, $L_t = \text{thickness of layer}$

Equation 4. Transmission coefficient for normal incidence case for a water bound panel.

The transmission coefficient is related to the insertion loss as follows

$$\text{Insertion Loss} = 10 \log_{10} [1 / \Gamma] = 10 \log_{10} [1 + .25([(\rho_2 c_2 / \rho_1 c_1) - (\rho_1 c_1 / \rho_2 c_2)]^2 \sin^2 k_2 L_t)]$$

Equation 5. Insertion Loss for normal incidence case of a water bound panel.

Inspection of Equation 5 reveals the indicators mentioned above. Namely, closely matched materials cause the $[(\rho_2 c_2 / \rho_1 c_1) - (\rho_1 c_1 / \rho_2 c_2)]$ term to approach zero, and likewise, $k_2 L$ products near $n \pi/2$ for $n=0,1,2,3\dots$ cause the sin term to vanish. Both have the effect of causing insertion loss to approach zero which corresponds to “perfect” transmission of the acoustic signal. On the other hand, the insertion loss goes to infinity as Γ approaches zero, with the physical interpretation in this case that little sound is allowed to pass through the material. Figure 3 demonstrates this point.

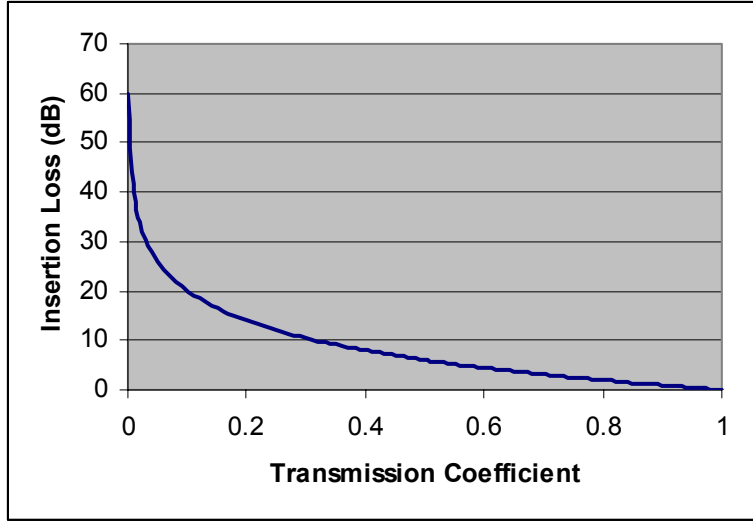


Figure 3. Insertion loss v transmission loss

Such results are useful in the idealized case of pure normal plane wave incidence. The more common case is wave incidence that is not strictly normal, and in such instances, a shear wave is generated in the solid because points along the water-solid interface are *not* excited in phase. For the off-normal incidence case, a more detailed approach that requires an understanding of stress tensors is necessary.

B. MULTI-LAYER NON-NORMAL INCIDENCE

1. Stress/Strain Wave Propagation

Waves in solids can be described as propagations of stress and strain within the material. Officer [8] provides a detailed derivation of the governing wave equation in solids. Brekhovskikh [9] expands this treatment by considering wave propagation through multi-layered solids. In both references, fundamental concepts of stress and strain are required as groundwork in the equation derivation. In the following, a short derivation of the governing equations is given.

Stress (T) is defined as the force acting on a given area (δA) divided by that area.

$$T = f/\delta A$$

Equation 6. Stress (T) definition

The stress state at a point in a continuum can be resolved into three traction vectors (t^1, t^2, t^3), each acting on a differential area whose normal is one of the three axis.

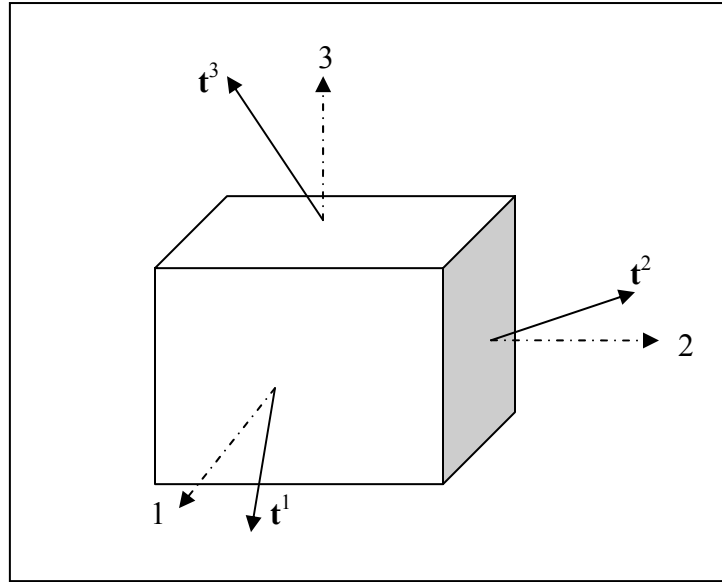


Figure 4. Traction vectors acting on orthogonal planes of a differential element from [10].

Each of these three tractions can then be further resolved into three orthogonal components. The resulting nine stress components are referred to using the following indicial (tensor) notation: T_{ij} , where i = index of the normal plane, and j is the coordinate component of the applied stress.

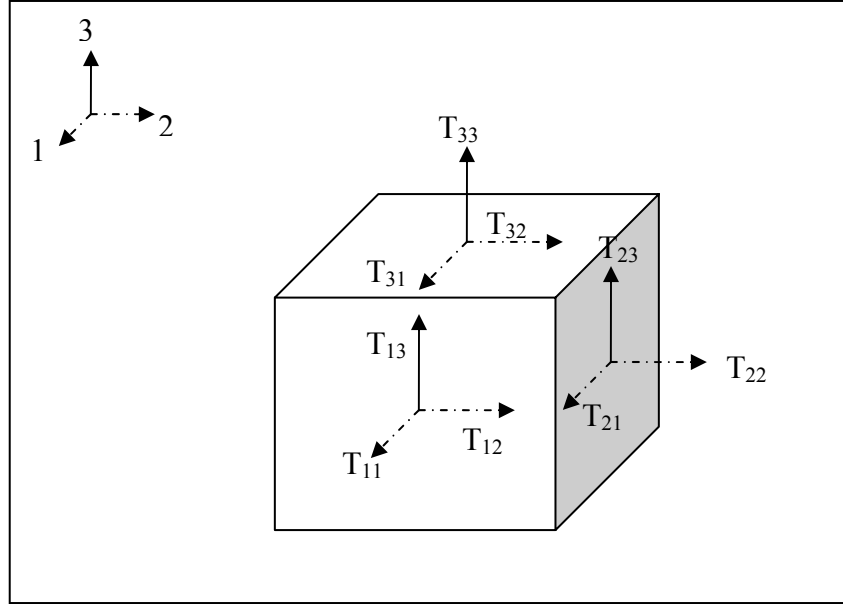


Figure 5. Traction vector components acting on a differential element from [10].

Before the equations of strain can be formulated, a definition for media displacement is required. Therefore, the displacement u_i identifies the displacement of a point in the i direction. Extensional strain can generally be defined as the relative change in position per unit distance. In a simple case, the change in axial length (δu_i) divided by the total length (δx). Shear strain is defined differently, as shown in figure below and in Equation 7.

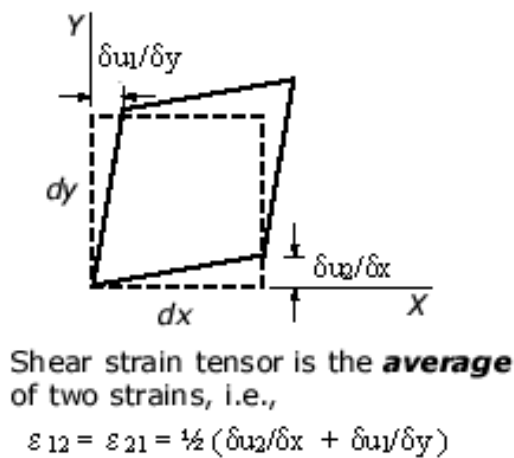


Figure 6. Shear strain definition from [10].

In a similar fashion to stress, the strains are referred to by indicial notation: ϵ_{ij} .

$$\begin{aligned}\epsilon_{11} &= \delta u_1 / \delta x & \epsilon_{22} &= \delta u_2 / \delta y & \epsilon_{33} &= \delta u_3 / \delta z \\ \epsilon_{12} &= \epsilon_{21} = \frac{1}{2} (\delta u_2 / \delta x + \delta u_1 / \delta y) \\ \epsilon_{13} &= \epsilon_{31} = \frac{1}{2} (\delta u_1 / \delta z + \delta u_3 / \delta x) \\ \epsilon_{32} &= \epsilon_{23} = \frac{1}{2} (\delta u_3 / \delta y + \delta u_2 / \delta z)\end{aligned}$$

Equation 7. Strain notation

The generalized form of Hooke's law is used to relate each of the nine stress components as a linear function of the nine components of strain, each multiplied by a 'stiffness' coefficient, c_{ijkl} . Officer's [8] derivation makes use of symmetries in stress and strain tensors identities and equilibrium considerations to reduce the generalized Hooke's law relations to six equations, displayed in Equation 8. A widely used enumeration scheme to reduce the number of subscripts on each term is given below.

$$\begin{aligned}T_1 &= c_{11} \epsilon_1 + c_{12} \epsilon_2 + c_{13} \epsilon_3 + c_{14} \epsilon_4 + c_{15} \epsilon_5 + c_{16} \epsilon_6 \\ T_2 &= c_{21} \epsilon_1 + c_{22} \epsilon_2 + c_{23} \epsilon_3 + c_{24} \epsilon_4 + c_{25} \epsilon_5 + c_{26} \epsilon_6 \\ T_3 &= c_{31} \epsilon_1 + c_{32} \epsilon_2 + c_{33} \epsilon_3 + c_{34} \epsilon_4 + c_{35} \epsilon_5 + c_{36} \epsilon_6 \\ T_4 &= c_{41} \epsilon_1 + c_{42} \epsilon_2 + c_{43} \epsilon_3 + c_{44} \epsilon_4 + c_{45} \epsilon_5 + c_{46} \epsilon_6 \\ T_5 &= c_{51} \epsilon_1 + c_{52} \epsilon_2 + c_{53} \epsilon_3 + c_{54} \epsilon_4 + c_{55} \epsilon_5 + c_{56} \epsilon_6 \\ T_6 &= c_{61} \epsilon_1 + c_{62} \epsilon_2 + c_{63} \epsilon_3 + c_{64} \epsilon_4 + c_{65} \epsilon_5 + c_{66} \epsilon_6\end{aligned}$$

Equation 8. Reduced form of generalized Hooke's law.

Nye [11] presents strain energy considerations that require $c_{mn} = c_{nm}$. When applied to Equation 8, this reduces the number of independent stiffness coefficients to 21.

Certain material classes allow these equations to be reduced even further if independence of one or more coordinate directions in the medium exists. The table below lists some material classes and the number of independent stiffness coefficients.

<i>Crystal Type</i>	<i>n_{sc}</i>	<i>Material Example</i>
Triclinic	21	Axinite
Monoclinic	13	Lithium Sulfate
Trigonal	6	Quartz
Hexagonal	5	Piezoelectric ceramic
Transversely isotropic	5	Unidirectional Layer in Composite Material
Isotropic	2	Steel, Engineering Polymers, Elastomers

Table 4. The number of independent stiffness coefficients (n_{sc}) for various crystal types.

Officer [8] reduces Equation 8 to two independent elastic constants for isotropic materials; λ and μ , known as Lamé's constants.

$$\begin{aligned}
 T_1 &= (2\mu + \lambda) \varepsilon_1 + \lambda \varepsilon_2 + \lambda \varepsilon_3 \\
 T_2 &= \lambda \varepsilon_1 + (2\mu + \lambda) \varepsilon_2 + \lambda \varepsilon_3 \\
 T_3 &= \lambda \varepsilon_1 + \lambda \varepsilon_2 + (2\mu + \lambda) \varepsilon_3 \\
 T_4 &= \mu \varepsilon_4 \\
 T_5 &= \mu \varepsilon_5 \\
 T_6 &= \mu \varepsilon_6
 \end{aligned}$$

Equation 9. Isotropic stress-strain equations.

2. Non-Normal, Multi-Layered, Unattenuated Case

For the case of a planar, liquid-solid interface, normal and tangential components of stress must be equal at that interface. However, since fluids support shear stress to a negligible degree, the tangential components of stress at the boundary are set to zero

while normal stress balances fluid pressure. A third boundary condition is continuity of the normal components of displacement at the interface. Conditions are summarized below:

- | |
|--|
| <ol style="list-style-type: none"> 1. Continuity of normal stress (T_3) across the boundary 2. Tangential stress (T_5) of zero at the boundary. 3. Continuity of normal displacement (u_3) |
|--|

Table 5. List of boundary conditions for general case of normal and non-normal incidence.

For two dimensional problems that are independent of the y coordinate, one need only consider the x - z plane of the medium. For any angle of incidence as shown in Figure 7, Brekhovskikh derives amplitudes of plane waves propagating through the layered material by repeated applications of the boundary conditions of Table 5 at every interface.

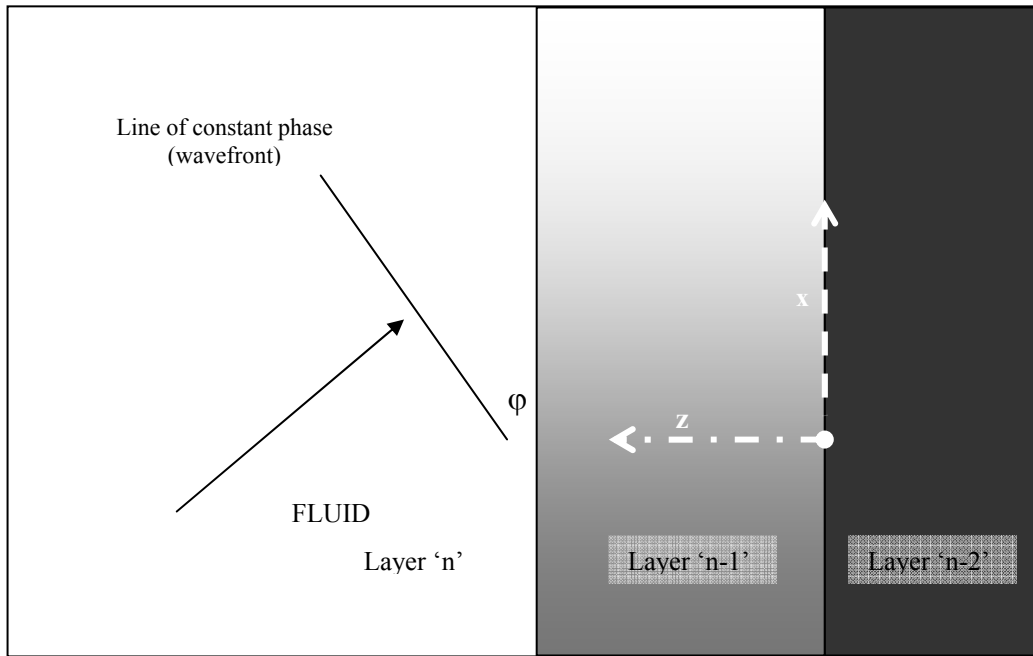


Figure 7. Wave propagation direction.

Brekhovskikh's derivation at a single interface leads to a set of linear equations presented in matrix form in Equation 10. It is important to note that the incident wave propagates in the negative z direction.

$$\begin{pmatrix} v_x^n \\ v_z^n \\ \omega T_3^n \\ \omega T_5^n / 2\mu \end{pmatrix} = \begin{pmatrix} jM \cos(Pz) & -M \sin(Pz) & Q \sin(Qz) & -jQ \cos(Qz) \\ -P \sin(Pz) & jP \cos(Pz) & jM \cos(Qz) & -M \sin(Qz) \\ -jK \cos(Pz) & K \sin(Pz) & 2\mu MQ \sin(Qz) & -j2\mu MQ \cos(Qz) \\ MP \sin(Pz) & -jMP \cos(Pz) & j((Q^2 - M^2)/2) \cos(Qz) & ((M^2 - Q^2)/2) \sin(Qz) \end{pmatrix} \begin{pmatrix} (\phi' + \phi'') \\ (\phi' - \phi'') \\ (\psi' + \psi'') \\ (\psi' - \psi'') \end{pmatrix}$$

Or, in short form:

$$[T^n] = [A^n] [S^n]$$

where:

$M_n = \kappa_n \sin \gamma_n = k_n \sin \phi_n = k_{n+1} \sin \phi_{n+1}$
 $P_n = k_n \cos \phi_n$
 $Q_n = \kappa_n \cos \gamma_n$
 $K = (M^2 \lambda + P^2 \lambda + 2\mu P^2)$
 $c_L = \text{Compressional wave speed}$
 $c_G = \text{Shear wave speed}$
 $k_n = \omega / c_L \text{ in layer 'n'}$
 $\kappa_n = \omega / c_G \text{ in layer 'n'}$
 $\gamma_n = \text{Shear wave propagation angle in layer 'n'}$
 $\phi_n = \text{Compressional wave propagation angle in layer 'n'}$

$\phi = \text{Compressional velocity potential}$
 $\phi' = \text{Incident}$
 $\phi'' = \text{Reflected}$
 $\psi = \text{Shear velocity potential}$
 $\psi' = \text{Incident}$
 $\psi'' = \text{Reflected}$

Equation 10. Matrix form of particle velocities and stress component equations in an isotropic layer, n.

A key concept used by Brekhovskikh in this multilayered scenario is that the $[S^n]$ do not have a z dependence, and therefore are constant through each layer. This means that stress at the top of the layer can be related to the stress at the bottom of a given layer by elimination of this common factor.

$$\begin{aligned} [T^{n-1}]_{z=\text{top of layer } n-1} &= [T^n]_{z=\text{bottom of layer } n} \\ [S^n]_{z=\text{anywhere in layer } n} &= [S^n]_{z=\text{bottom or top of layer } n} \end{aligned}$$

Equation 11. Continuity of displacements and tractions at the boundary.

Invertability of the matrix in Equation 10 is assumed in establishing a relationship between layers n and $n-1$, as below.

$$\begin{aligned} [T^n]_{z=\text{bottom of layer } n} &= [T^{n-1}]_{z=\text{top of layer } n-1} \\ [T^{n-1}]_{z=\text{top of layer } n-1} &= [A^{n-1}]_{z=\text{top of layer } n-1} [S^{n-1}], \text{ therefore} \\ [T^n]_{z=\text{bottom of layer } n} &= [A^{n-1}]_{z=\text{top of layer } n-1} [S^{n-1}], \text{ but} \\ [T^{n-1}]_{z=\text{bottom of layer } n-1} &= [A^{n-1}]_{z=\text{bottom of layer } n-1} [S^{n-1}], \text{ so} \\ [A^{n-1}]_{z=\text{bottom of layer } n-1}^{-1} [T^{n-1}]_{z=\text{bottom of layer } n-1} &= [S^{n-1}] \\ \Rightarrow [T^n]_{z=\text{bottom of layer } n} &= [A^{n-1}]_{z=\text{top of layer } n-1} [S^{n-1}] \\ &= [A^{n-1}]_{z=\text{top of layer } n-1} [A^{n-1}]_{z=\text{bottom of layer } n-1}^{-1} [T^{n-1}]_{z=\text{bottom of layer } n-1} \\ [T^n] &= [\Sigma^{n-1}] [T^{n-1}] \\ \Rightarrow [T^{n-1}] &= [\Sigma^{n-2}] [T^{n-2}] \\ [T^n] &= [\Sigma^{n-1}] [\Sigma^{n-2}] [T^{n-2}] \\ [T^n] &= [\Sigma^{n-1}] [\Sigma^{n-2}] \dots [\Sigma^1] [T^1] \\ \Rightarrow [T^n] &= [\Lambda] [T^1] \end{aligned}$$

Equation 12. Matrix form of recurrence relationship between isotropic layers n and 1 .

The Λ matrix in Equation 12 is a 4×4 matrix that is the product of $[\Sigma^{n-1}] \dots [\Sigma^1]$. Finally, for the special case of isotropic material bounded by water, Brekhovskikh derives a pressure ratio, which can be related to the intensity transmission coefficient, which in turn can subsequently be used to determine insertion loss at both normal and non-normal angles of incidence.

$$\text{Insertion Loss} = 10 \log_{10} [1 / \Gamma]$$

$$\Gamma = [-2 P_n \omega^2 \rho_1 / (H1+H2)]^2$$

where :

$$\begin{aligned} \rho_1 &= \text{Density in layer 1 (seawater)} & \rho_n &= \text{Density in layer n} \\ H1 &= P_n [P_1 Y3 - \omega \rho_1 \omega Y4] & H2 &= -\rho_n \omega^2 [P_1 Y1 - \omega \rho_1 \omega Y2] \\ Y1 &= [(-1/\Lambda_{41}) \quad \Lambda_{42} \quad \Lambda_{21} + \Lambda_{22}] & Y2 &= [(-1/\Lambda_{41}) \quad \Lambda_{43} \quad \Lambda_{21} + \Lambda_{23}] \\ Y3 &= [(-1/\Lambda_{41}) \quad \Lambda_{42} \quad \Lambda_{31} + \Lambda_{32}] & Y4 &= [(-1/\Lambda_{41}) \quad \Lambda_{43} \quad \Lambda_{31} + \Lambda_{33}] \end{aligned}$$

Equation 13. Insertion loss using intensity transmission coefficient for multi-layered, water bound, isotropic material at normal and non-normal angles of incidence.

3. Non-Normal, Multi-Layer, Attenuated Case

Equation 5 and Equation 13 neglect attenuation of the pressure wave as it propagates through the layer. Brekhovskikh's approach simply multiplies potentials by decay terms, such as $\exp(-\xi z)$, where ξ is the attenuation term and z is the spatial variable. The shear and compressional decay terms, ξ_G and ξ_L , are defined by Capps [12] below in terms of the loss properties in the material, characterized by the 'tan δ ' metric.

$$\xi_G = \text{SQRT} [\rho \omega^2 ((1 + \tan^2 \delta_G)^{1/2} - 1) / 2 \mu' (1 + \tan^2 \delta_G)]$$

$$\xi_L = \text{SQRT} [\rho \omega^2 ((1 + \tan^2 \delta_L)^{1/2} - 1) / 2L' (1 + \tan^2 \delta_L)]$$

$$L = (\lambda + 2\mu)$$

$$L' = \text{Real part of } L$$

$$L'' = \text{Loss part of } L$$

$$\tan \delta_L = \text{loss tangent associated with } L = L''/L'$$

$$\tan \delta_G = \text{loss tangent associated with } \mu = \mu''/\mu'$$

Equation 14. Compression and shear decay term definition.

Since the incident wave is traveling in the negative z direction, the resulting wave propagation takes the following form, using the variables from Equation 10:

$$\phi = [\phi' \exp (jPz -\xi_L (d-z)) + \phi'' \exp (- jPz-\xi_L z)] \exp (jM-\xi_L x)$$

$$\phi = [\phi' \exp (jPa z -\xi_L d) + \phi'' \exp (- jPa z)] \exp (jMa x)$$

$$\text{where: } Pa = P -j\xi_L , \quad Ma = M -j\xi_L$$

$$\psi = [\psi' \exp (jQz -\xi_G (d-z)) + \psi'' \exp (- jQz-\xi_G z)] \exp (jM-\xi_G x)$$

$$\psi = [\psi' \exp (jQa z -\xi_G d) + \psi'' \exp (- jQa z)] \exp (jMa x)$$

$$\text{where: } Qa = Q -j\xi_G$$

Equation 15. Velocity potentials equation for the attenuated wave case.

When attenuation exists, a modified set of equations, based on the same approach used to develop Equation 10, can be derived. Equation 16 displays these modified equations, based on the modified potentials of Equation 15, in matrix form. It can be seen that the potential sums shown in Equation 10 are replaced by individual potentials for the upward and downward traveling compressional and shear waves, scaled by decay terms.

$$\begin{pmatrix} V_x \\ V_z \\ \omega T_3 \\ \omega T_5 \end{pmatrix} = j \begin{pmatrix} Ma e1 & Ma e2 & -Qa e3 & Qa e4 \\ Pa e1 & -Pa e2 & Ma e3 & Ma e4 \\ -Ka e1 & -Ka e2 & -2\mu MQa e3 & 2\mu MQa e4 \\ -2\mu Pa Ma e1 & 2\mu Pa Ma e2 & -\mu (Ma^2 - Qa^2) e3 & -\mu (Ma^2 - Qa^2) e4 \end{pmatrix} \begin{pmatrix} \phi' \\ \phi'' \\ \psi' \\ \psi'' \end{pmatrix}$$

Or, in short form:

$$[T] = j [A2] [S2]$$

where:

$$Ka = (Ma^2\lambda + Pa^2\lambda + 2\mu Pa^2)$$

$$\begin{aligned}
 e1 &= \exp(jPa_z - \xi_L d) \\
 e2 &= \exp(-jPa_z) \\
 e3 &= \exp(jQa_z - \xi_G d) \\
 e4 &= \exp(-jQa_z)
 \end{aligned}$$

Equation 16. Matrix form of linear equations with upward and downward potentials separated.

A recurrence relationship similar to that described in Equation 12 also exists for the attenuated case.

$$\begin{aligned}
[T^{n-1}_{z=\text{bottom of layer } n-1}] &= [A2^{n-1}_{z=\text{bottom of layer } n-1}] [S2^{n-1}] \\
[S2^{n-1}] &= [A2^{n-1}_{z=\text{bottom of layer } n-1}]^{-1} [T^{n-1}_{z=\text{bottom of layer } n-1}] \\
[T^{n-1}_{z=\text{top of layer } n-1}] &= [A2^{n-1}_{z=\text{top of layer } n-1}] [S2^{n-1}] \\
[T^{n-1}_{z=\text{top of layer } n-1}] &= \\
[A2^{n-1}_{z=\text{top of layer } n-1}] [A2^{n-1}_{z=\text{bottom of layer } n-1}]^{-1} [T^{n-1}_{z=\text{bottom of layer } n-1}] \\
[T^n_{z=\text{bottom of layer } n}] &= [T^{n-1}_{z=\text{top of layer } n-1}] \\
[T^n_{z=\text{bottom of layer } n}] &= \\
[A2^{n-1}_{z=\text{top of layer } n-1}] [A2^{n-1}_{z=\text{bottom of layer } n-1}]^{-1} [T^{n-1}_{z=\text{bottom of layer } n-1}] \\
[T^n_{z=\text{bottom of layer } n}] &= [\Sigma^{n-1}] [T^{n-1}_{z=\text{bottom of layer } n-1}] \\
[T^{n-1}] &= [\Sigma^{n-2}] [T^{n-2}] \\
[T^n] &= [\Sigma^{n-1}] [\Sigma^{n-2}] \dots [\Sigma^1] [T^1] \\
\Rightarrow [T^n] &= [\Lambda] [T^1]
\end{aligned}$$

Equation 17. Matrix form of recurrence relationship between isotropic layers n and 1 for the attenuated case.

The intensity transmission coefficient can be determined using a similar approach, modified to account for the matrix differences between Equation 10 and Equation 15, to that used by Brekovskikh in the non-attenuating case referenced above. Again, the insertion loss metric is related to the transmission coefficient. The final equation is shown below.

$$\text{Insertion Loss} = 10 \log_{10} [1 / \Gamma_a]$$

$$\Gamma_a = [-2 P_{a,n} \rho_1 K_{a,n} / \rho_n (H3 + H4)]^2$$

where :

$K_{a,n}$ = K_a in layer n

$P_{a,n}$ = P_a in layer n

$P_{a,1}$ = P_a in layer 1

$$H3 = -K_{a,n} [-Y1i P_{a,1} + \rho_1 \omega^2 Y2i]$$

$$H4 = -P_{a,n} [-Y3i P_{a,1} + \rho_1 \omega^2 Y4i]$$

$$Y1i = [(-1/\Lambda_{i41}) \Lambda_{i42} \Lambda_{i21} + \Lambda_{i22}]$$

$$Y2i = [(-1/\Lambda_{i41}) \Lambda_{i43} \Lambda_{i21} + \Lambda_{i23}]$$

$$Y3i = [(-1/\Lambda_{i41}) \Lambda_{i42} \Lambda_{i31} + \Lambda_{i32}]$$

$$Y4i = [(-1/\Lambda_{i41}) \Lambda_{i43} \Lambda_{i31} + \Lambda_{i33}]$$

Equation 18. Insertion loss with attenuation using intensity transmission coefficient for multi-layered, water bound, isotropic material at normal and non-normal angles of incidence.

Since literature values for λ are uncommon, it can be calculated using Young's modulus (E) and μ . In turn, μ is found given E and ν according to Equation 19 from Loeser [13]. Due to the lack of experimental data, a simplification is made concerning Poisson's ratio that assumes it is a real number: $\nu'' = 0$ so $\nu^* = \nu'$.

$$\begin{aligned} \mu^* &= E^* / 2 (1 + \nu^*) \\ \mu^* &= E^* / 2 (1 + \nu') \\ \mu' (1 + j \tan \delta_G) &= E' (1 + j \tan \delta_E) / 2 (1 + \nu') \\ \rightarrow (\tan \delta_G) &= (\tan \delta_E) \end{aligned}$$

Equation 19. Relationship between shear modulus, Young's modulus and Poisson's ratio for the case of $\nu'' = 0$.

Using Equation 19 and the definition of λ in terms of E and ν shown in Loeser, λ^* can be calculated as follows:

$$\begin{aligned}\lambda^* &= \nu' E^* / (1 + \nu') (1 - 2\nu') \\ 2\mu^* &= E^* / (1 + \nu') \\ (\lambda^* + 2\mu^*) &= (E^* / (1 + \nu')) [\nu' / (1 - 2\nu') + 1]\end{aligned}$$

Equation 20. Relationship between compressional modulus, Young's modulus and Poisson's ratio for the case of $\nu'' = 0$.

Since signal decay is primarily associated with the materials' elastic moduli, introduction of complex terms affects the magnitudes of propagation speeds in the material. Capps defines these speeds using loss tangents as follows:

$$\begin{aligned}c_G &= \text{SQRT} [2\mu' (1 + \tan^2 \delta_G) / \rho ((1 + \tan^2 \delta_G)^{1/2} + 1)] \\ c_L &= \text{SQRT} [2L' (1 + \tan^2 \delta_L) / \rho ((1 + \tan^2 \delta_L)^{1/2} + 1)]\end{aligned}$$

Equation 21. Sound speed equations for lossy material.

Using Equation 19 and Equation 20, Equation 14 and Equation 21 can be rewritten in terms of complex Young's and Poisson's moduli E and ν .

$$\begin{aligned}c_L &= \text{SQRT} ([2 (E' / (1 + \nu')) [\nu' / (1 - 2\nu') + 1] / \rho] [TD / (TD^{1/2} + 1)]) \\ c_G &= \text{SQRT} ([2 / (E' / 2 (1 + \nu')) \rho] [TD / (TD^{1/2} + 1)]) \\ \xi_G &= \text{SQRT} ([\rho \omega^2 / 2 (E' / 2 (1 + \nu'))] [(TD^{1/2} - 1) / TD]) \\ \xi_L &= \text{SQRT} ([\rho \omega^2 / 2 (E' / (1 + \nu')) [\nu' / (1 - 2\nu') + 1]] [(TD^{1/2} - 1) / TD]) \\ TD &= (1 + \tan^2 \delta_E)\end{aligned}$$

Equation 22. Compressional and shear sound speeds and decay terms expressed as functions of E and ν .

THIS PAGE INTENTIONALLY LEFT BLANK

III. MEASUREMENTS AND MODELS

A. MEASUREMENTS

To verify the theoretical models discussed in previous sections, experimental measurements were made on panels of several materials listed in Table 2. These measurements were made at several different open water facilities using identical measurement protocols.

Insertion loss was calculated according to Equation 3 using sound pressure level (SPL) measurements. An incident signal was produced by a calibrated reference standard projector, with and without a panel in the acoustic signal path between the projector and a calibrated reference standard hydrophone. The rotator shaft is used to position the panel such that a plane wave from the projector strikes the panel at varying angles of incidence. The setup is shown below in Figure 8.

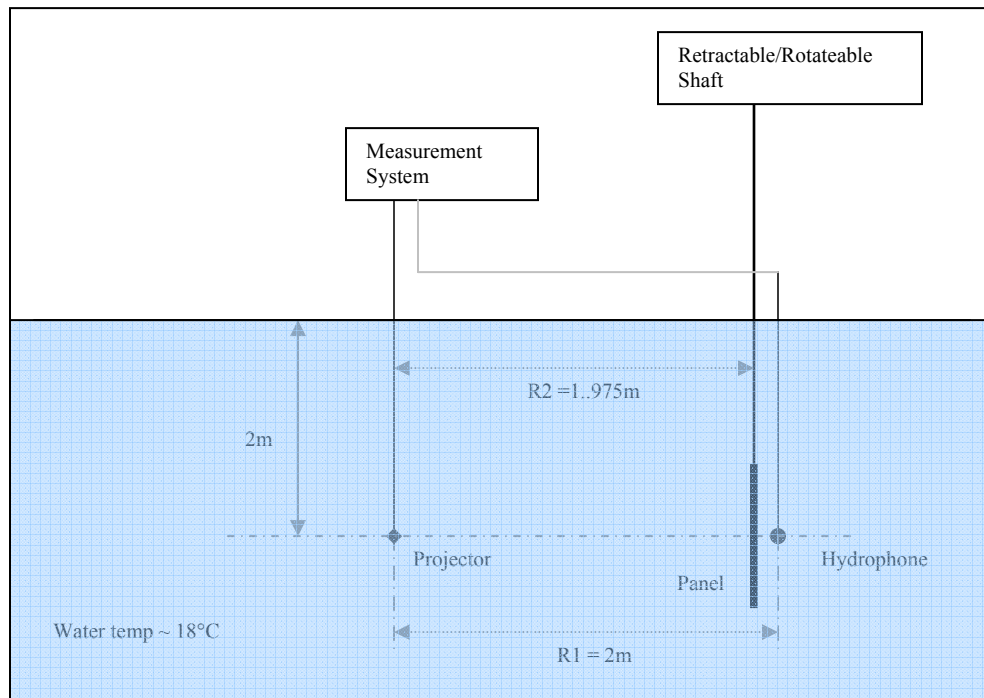
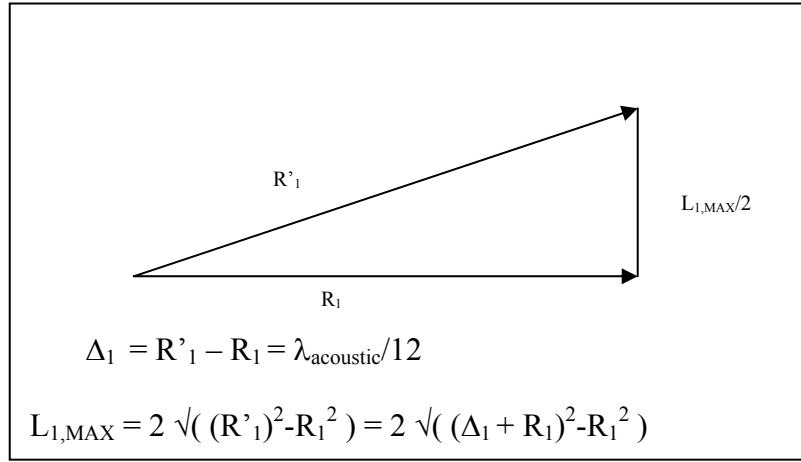


Figure 8. Acoustic Measurement Setup

In practice, two issues must be addressed to assure test setup and panel sizes are sufficient to address geometric influences affecting measurement quality. The first of these is the fact that the wavefront incident on the panel is not planar, but spherical. The issue can be mitigated by applying the criterion that the maximum dimension of the hydrophone used to measure the signal be such that the incident signal at the edge and the center of the hydrophone be no more than 30° out of phase, or $\lambda_{\text{acoustic}}/12$. This requirement forces a maximum hydrophone length ($L_{1,\text{MAX}}$) defined by Equation 23.



Equation 23. Minimum panel length for plane wave assumption.

The second geometric issue is an effect called ‘edge diffraction’ [3]. Using Figure 8 and Figure 9, $R_3 = R_1 - R_2$. The distance from the edge of the panel to the center of the hydrophone is shown in

Figure 9 as R_3' . The panel must be large enough such that the difference between R_3' and R_3 is large enough to allow a signal to be sampled before edge diffraction signal arrives. Since the reference hydrophone requires 2-3 cycles to reach steady state, this criterion is set at four wavelengths (minimum) to allow one full cycle to sample.

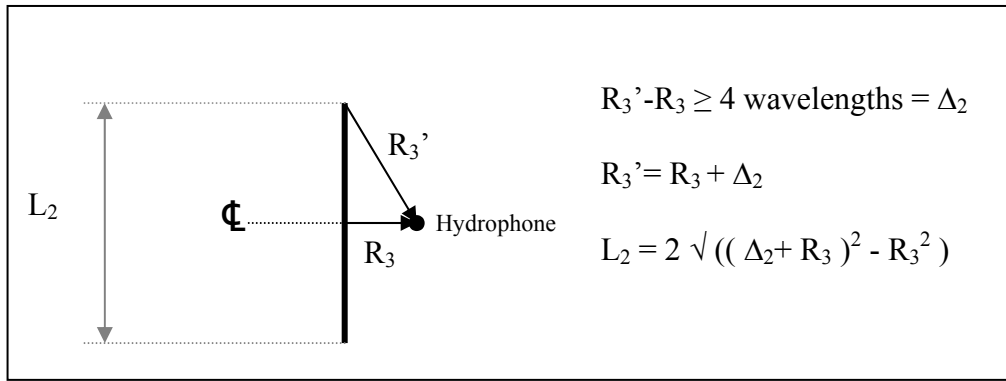


Figure 9. Minimum panel to address edge diffraction.

Figure 10 shows that hydrophone length should not be larger than 0.09m (9cm). The H-52 type hydrophone (Length = 5cm) is the largest used in these measurements and easily meets the criteria. The line marked 'L2' in Figure 10 represents the minimum panel length required as a function of frequency. The largest panel size required is ~.29m (11 inches) at the low end of the band.

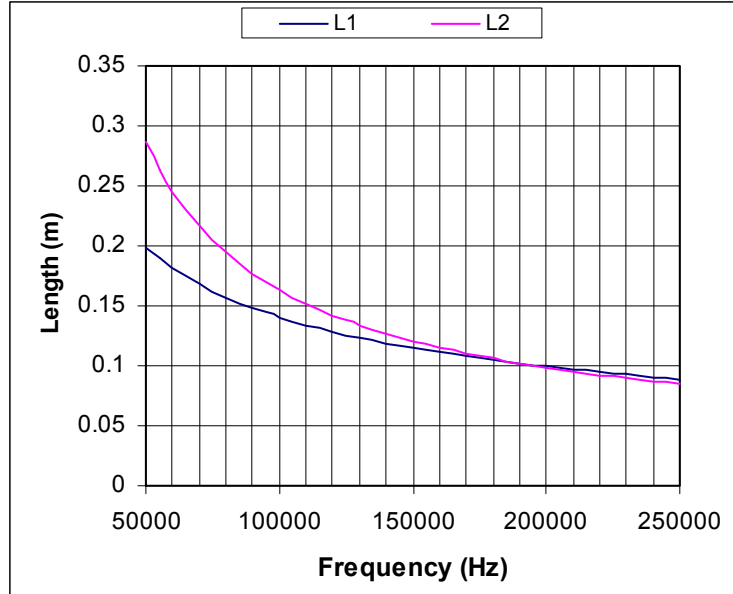


Figure 10. Minimum required panel length L_2 and maximum hydrophone length L_1 .

Both transducer and hydrophone have accuracies within $\pm 0.1\text{dB}$, in ideal conditions. Two measurements are required to establish the insertion loss value. Therefore, total inaccuracies in measured data could be as large as $\pm 0.4\text{dB}$.

B. MODEL

Equation 5 , Equation 13 and Equation 18 , derived in the previous section for isotropic layers bounded by water, represent three levels of insertion loss models with increasing levels of complexity; Equation 5 for the simplest case of normal incidence/ no attenuation, Equation 13 for non-normal incidence without attenuation, and Equation 18 for non-normal incidence that includes attenuation. Each, hereafter referred to as Model 1, 2, and 3, respectively, can be used as the basis equation for an insertion loss model that require user input of the following variables:

1. Number of layers
2. Angle of Incidence (Equation 13 and Equation 18)

And for each layer:

3. Young's Modulus (E)
4. Poisson's ratio (ν)
5. Young's $\tan \delta$ (Equation 18)
6. Layer thickness

Although it is not readily obvious, a quick comparison between methods for the case of a single layer of non-attenuating steel that is one cm thick, with a normally incident acoustic plane wave, produces identical results. The MATLAB code for model 3 is included in the Appendix.

To further validate Model 3, it is also checked against cases of single layered, isotropic materials at various incidence angles and levels of attenuation. Material property inputs used to test the model are listed in Table 6.

Density and Poisson's ratios are found in multiple sources for the items listed in the table below. The dynamic properties, Young's (Storage) modulus and $\tan \delta$, vary significantly with temperature and frequency. Little data for the specific materials and frequency ranges used in this thesis can be found in the literature. In the case of

polyurethane, Capps [12] provides $\tan \delta$ measurements versus a scaled frequency across a broad frequency band. The scaling coefficient accomplishes a $\tan \delta$ shift at temperatures away from the reference temperature. Specific moduli and $\tan \delta$ measurements on Noryl plastic were available [14]. On the other hand, nylon 6 moduli and $\tan \delta$ values were estimated from available data at frequencies outside the range of the thesis bounds.

<i>Material</i>	<i>Density(g/cc)</i>	<i>Young's Modulus (GPa)</i>	<i>Tan δ</i>	<i>Poisson's Ratio (ν)</i>
Plastic ² (Noryl EN-265)	1.08	2.62	0.029	0.38
Plastic ³ (Cast Nylon 6)	1.12	4.14	0.023	0.38
Steel (A36)	7.7	207	~0	0.29
Polyurethane (PR 1574)	1.03	0.200	0.150	0.49

Table 6. Physical properties for single layer, isotropic materials used in the test cases.

C. NORMAL INCIDENCE MODELS AND MEASUREMENTS

In Figure 11 and Figure 12, the model results and the measured data are plotted for the two plastic material cases subject to normal incidence acoustic waves. The agreement between the model and the measured data is good. The fact that the measured data shows a sinusoidal shape of a similar period as the model data indicates the sound speed and density estimates are close to the actual. The attenuation values are also validated, based on the similar linear ‘DC bias’ evident in both the model and measured cases.

² Noryl EN-265 plastic dynamic properties determined from sample measurements at various temperatures [14].

³ Cast Nylon 6 dynamic properties are estimates. Modulus is estimated from sound speed measurements made by Underwater Sound Reference Division (USRD) along with density and Poisson's ratio. Tan δ value estimate is made using ultrasonic (2.25MHz) measurements.

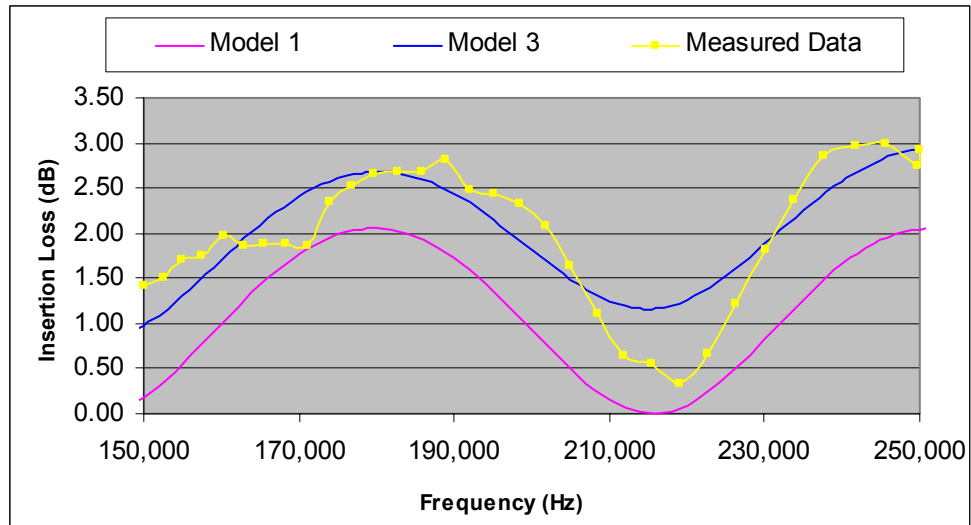


Figure 11. Insertion loss of 1.905cm cast Nylon 6 panel at normal incidence.

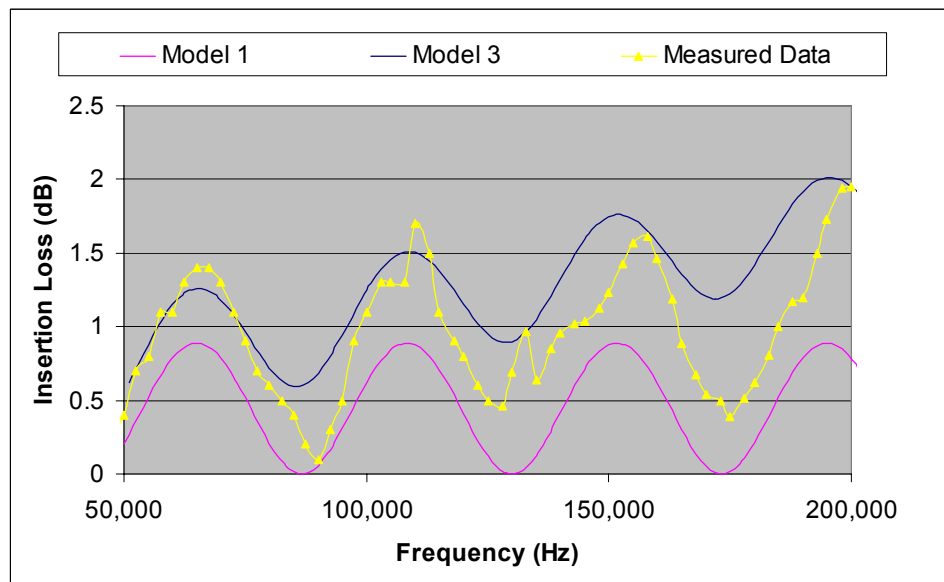


Figure 12. Insertion loss of 2.54cm Noryl EN-265 panel at normal incidence.

Normal incidence steel plate measurements shown in Figure 13 indicate that, although there is fluctuation in the measurement, the model to measurement match is good. This is evident when the following is considered. When insertion loss is high, as in this case of $> 17\text{dB}$, the received signal has an increased susceptibility to measurement system noise, both electronic and acoustic. Electronic noise is related to measurement

system equipment and signal to noise ratio. Acoustic ‘noise’ is the result of small, otherwise insignificant, reflections from various scatterers located, unavoidably, within such range as to coherently sum with the incident signal. In this case of the steel plate, the periodicity of the ripple in Figure 13 suggests the measured signal contained a reflection from a nearby (0.05m) scatterer, likely the hydrophone fixture. If the steel panel data points are least squares fit to a 3rd order polynomial, the agreement between measurements and model greatly improves, as shown in Figure 14.

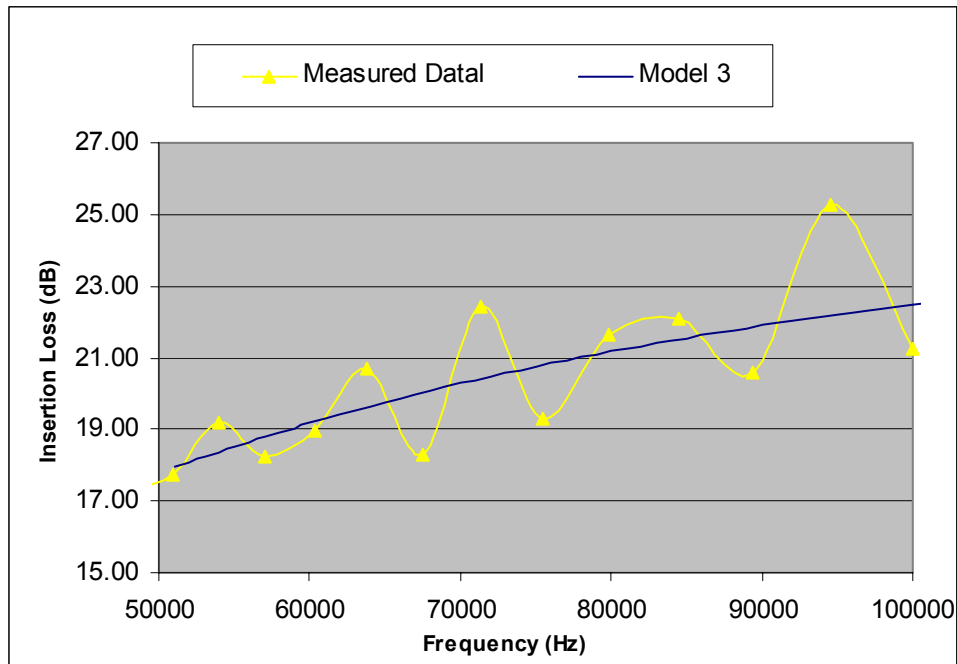


Figure 13. Insertion loss of 1.0cm A36 carbon steel plate at normal incidence.

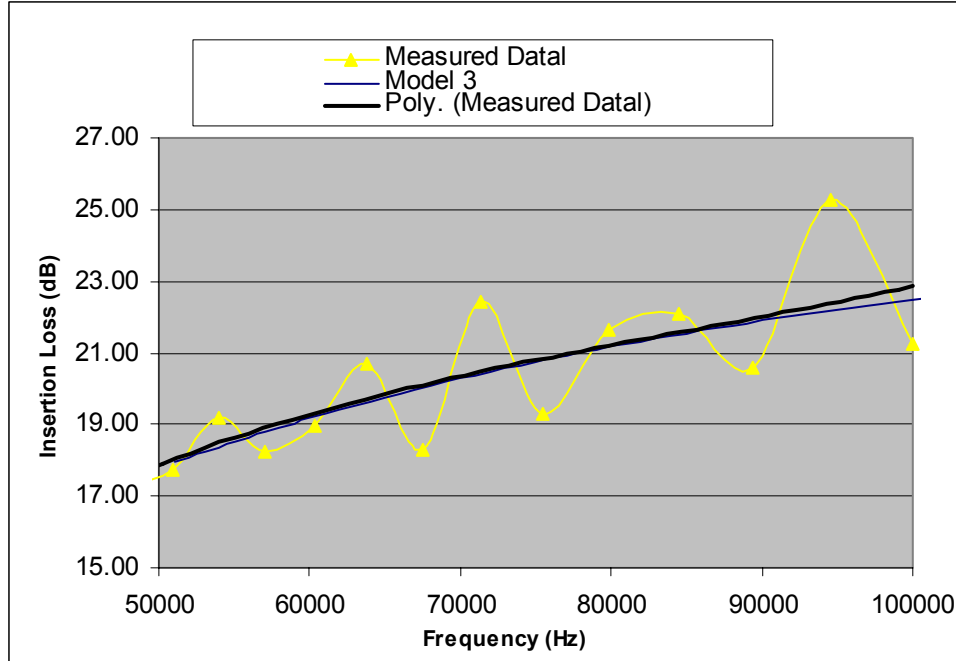


Figure 14. Insertion loss of 1.0cm A36 carbon steel plate at normal incidence with measured data points fit with a 3rd order polynomial curve.

Finally, the case of a polyurethane panel is presented below in Figure 15. Note that the insertion loss level is very low, relative to the steel plate case. The measured data agree very well with model 1, which does not include an estimate on attenuation in the material. Model 3, on the other hand, does include the effect of wave attenuation through the material based on an attenuation value given by Capps [12]. Since model 1 and model 3 inputs, with the exception of attenuation, are identical, it's clear that the disagreement between model 3 and the measured data is based on the attenuation input. If the attenuation value is lowered by an order of magnitude, agreement between model 3, model 1 and the measured data greatly improves, as demonstrated by Figure 16. As mentioned previously, there is scarce measured attenuation data in the literature for the specific frequency range and material used in this thesis. As such, the attenuation input given by Capps and used for the polyurethane panel model could not be verified by a second literature source and its accuracy, based on the measurements done here, is suspect.

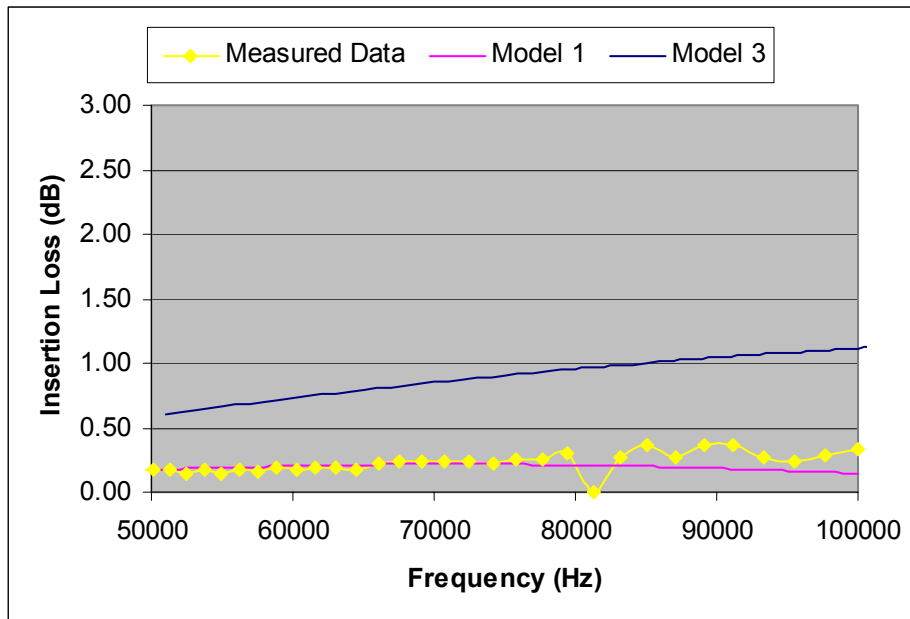


Figure 15. Insertion loss of 0.635cm thick PR-1574 panel at normal incidence.

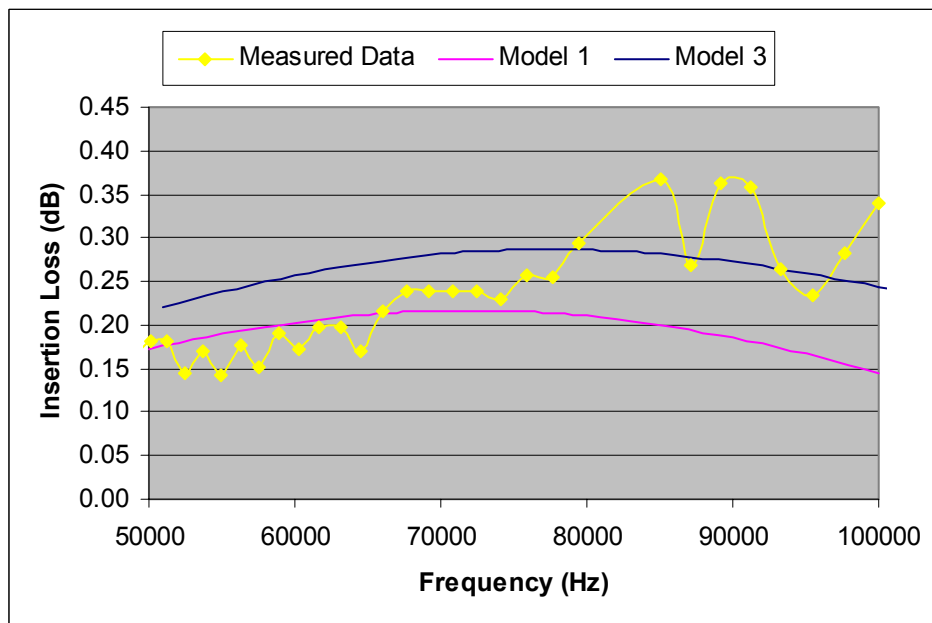


Figure 16. Insertion loss of 0.635 cm thick PR-1574 panel with low (0.015) loss tangent.

D. NON-NORMAL INCIDENCE MODELS AND MEASUREMENTS

Equation 13 (model 3) is capable of calculating insertion loss for non-normal incidence cases as well. As in section C above, insertion loss measurements were made on panels of several material types at prescribed incidence angles, and are shown below compared to experimental measurements.

The case of the Nylon panel at non-normal incidence is shown in Figure 17. An insertion loss peak at 160 kHz in Figure 17 is significantly overestimated by the model, indicating that the model input values are still not exact. Since the normal incidence model-to-measurement match was good and hence validated the values used for longitudinal sound speed and density, this spike in the insertion loss data likely indicates the Nylon shear estimates require update.

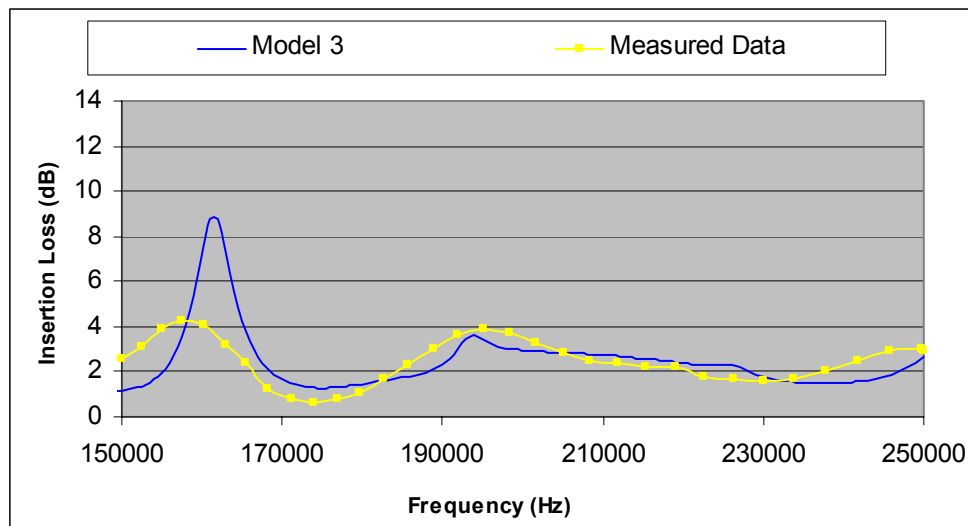


Figure 17. Insertion loss of 1.905cm thick Cast Nylon 6 panel at 15° incidence.

The case of a steel plate at non-normal incidence is shown in Figure 18. Despite measurement fluctuation similar to that seen in the normal incidence case, and attributed to the same cause, the match between the model and the measured data is considered good, indicating shear estimates are validated.

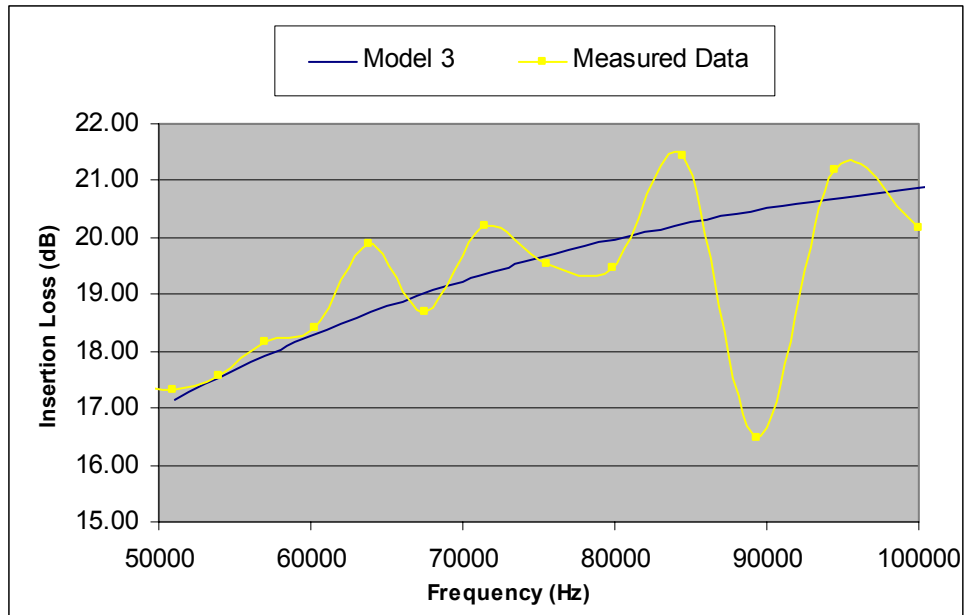


Figure 18. Insertion loss of 1.0cm thick A36 carbon steel panel at 20° incidence.

Once again, the polyurethane panel measurement results, plotted in Figure 19, have the largest deviation from model 3. This non-normal incidence case shows results similar to the normal incidence case and further supports the hypothesis of an inaccurate attenuation input.

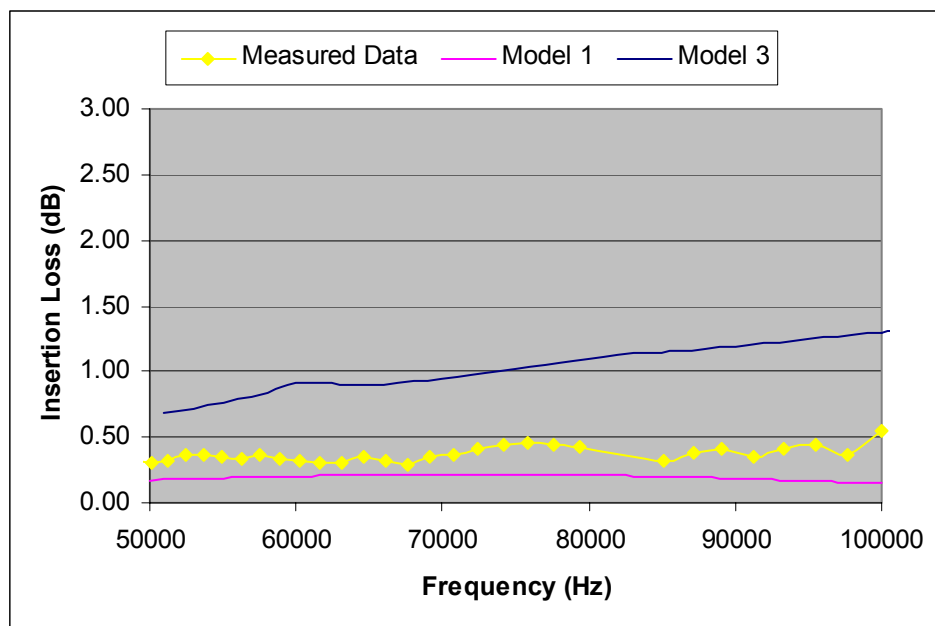


Figure 19. Insertion loss of 0.635cm thick PR1574 panel at 30° incidence.

IV. COMMENTS AND DISCUSSION

A. DESIGN IMPROVEMENT

Although model 3 is valid for multi-layered materials, no actual panels of such are available for test and subsequent model comparison. However, a comparison of several layered models provides insight into the effect of each layer.

A benefit of using a layered approach is the ability to determine an effective bending stiffness. Most acoustic windows are secured to the hull structure such that the window can be considered a plate with fixed edges. Structural loads carried by the window limit the resulting bending displacement criteria to ensure geometric stability and equipment clearances are maintained. Displacement and bending rigidity, D , are classically related by the plate equation given in Equation 24.

$$\begin{aligned} p &= \nabla^2 D \nabla^2 w \\ D &= \text{bending rigidity} \\ w &= \text{displacement} \\ p &= \text{pressure load} \end{aligned}$$

Equation 24. Classical (Kirchoff) plate bending equation

$$\begin{aligned} D &= \frac{1}{3} \sum_{k=1}^N (E_k / (1 - \nu_k^2)) (z_k^3 - z_{k-1}^3) \\ k &= \text{Layer number} \end{aligned}$$

Equation 25. Bending rigidity equation for plates

Equation 25 is based on the work by Jones [15] which uses Kirchoff's thin plate assumptions, generally considered to be satisfied for plates with lateral dimensions at

least 20 times the thickness.⁴ The bending rigidity of a plate with n layers can be broken into n separate integrals and summed to determine D for the composite section. For example, if PR-1574 polyurethane, 1.905cm thick, is sandwiched between two .0635cm thick Aluminum plates, the effective bending rigidity is calculated by breaking the integral into three parts, D_1 - D_3 , and summing the terms.

For this case, as shown in Table 7 using the inputs listed in Table 8, D for the composite section increases by a factor of ~ 50 relative to a single layer of equal thickness of PR-1574.

D_1	4834.00
D_2	151.63
D_3	4834.00
$D_{\text{Total for Composite Section}}$	9819.63
$D_{\text{Constant section}}$	184.02

Table 7. Bending rigidity for an ALUM-PR1574-ALUM composite section and a PR1574 constant section for a given thickness.

<i>Material</i>	<i>Density (g/cc)</i>	<i>Young's Modulus (GPa)</i>	<i>Tan δ</i>	<i>Layer Thickness (cm)</i>	<i>Poisson's Ratio</i>
Layer 1	2.7	70	.002	.0635	0.33
Layer 2	1.03	0.20	.1	1.905	0.49
Layer 3	2.7	70	.002	.0635	0.33

Table 8. Layered material 1:ALUM-PR1574-ALUM.

The discussion above highlights the structural benefits to a layered multi-media approach. The acoustic performance can be evaluated using Table 8 inputs for a 3 layered system. The insertion loss is calculated for various angles using model 3 and shown in Figure 20.

⁴ Plates not meeting the dimension criteria and/or those with relatively low shear rigidity require 'thick' plate analysis to determine bending displacements. See Reissner [16].

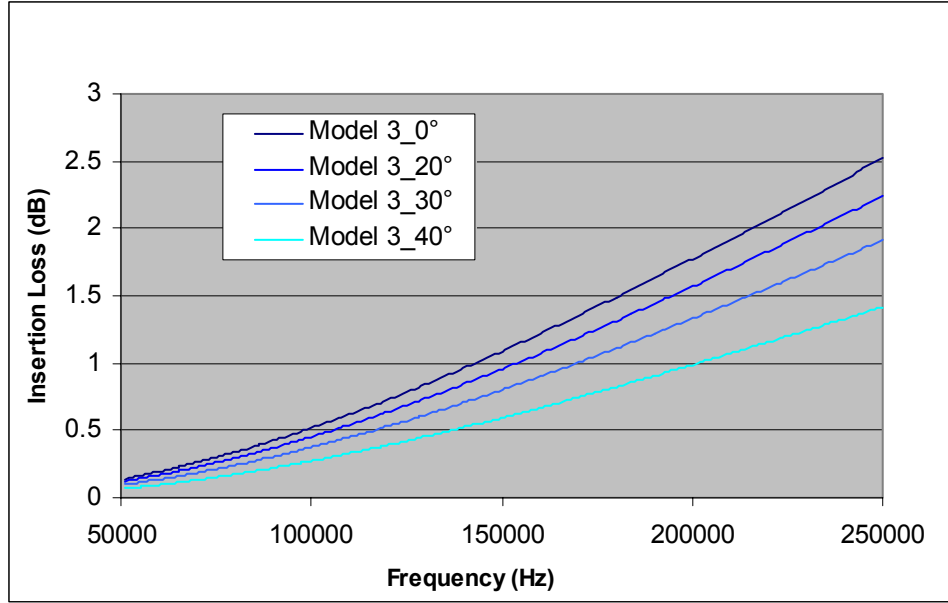


Figure 20. Model 3 insertion loss prediction of ALUM-PR1574-ALUM 'sandwich' composite with properties as shown in Table 8.

Insertion loss of the ALUM-PR1574-ALUM composite section shown in Figure 20 increases across the band to exceed the benchmark of 2dB at only a small portion of the high end of the band for the angles shown. A contour plot of the same data, shown in Figure 21, provides a better display of the data and reveals that this benchmark is also violated in a larger part of the frequency band at $\sim 16^\circ$ angle of incidence. The sharp increase in insertion loss at this angle can be shifted in angle by modifying the modulus of layers 1 and 3, as evidenced in Figure 22 where the modulus is lowered by $\sim 20\%$. Lowering layer 1 and 3 modulus by a full order of magnitude (to 7GPa) results in the complete elimination of the insertion loss peak, as seen in Figure 23. This suggests that the sharp differences in modulus, and hence acoustic impedance, between the outer layers (1 and 3) and the core layer (layer 2) produce internal reflections that interfere with the sound transmission through the material.

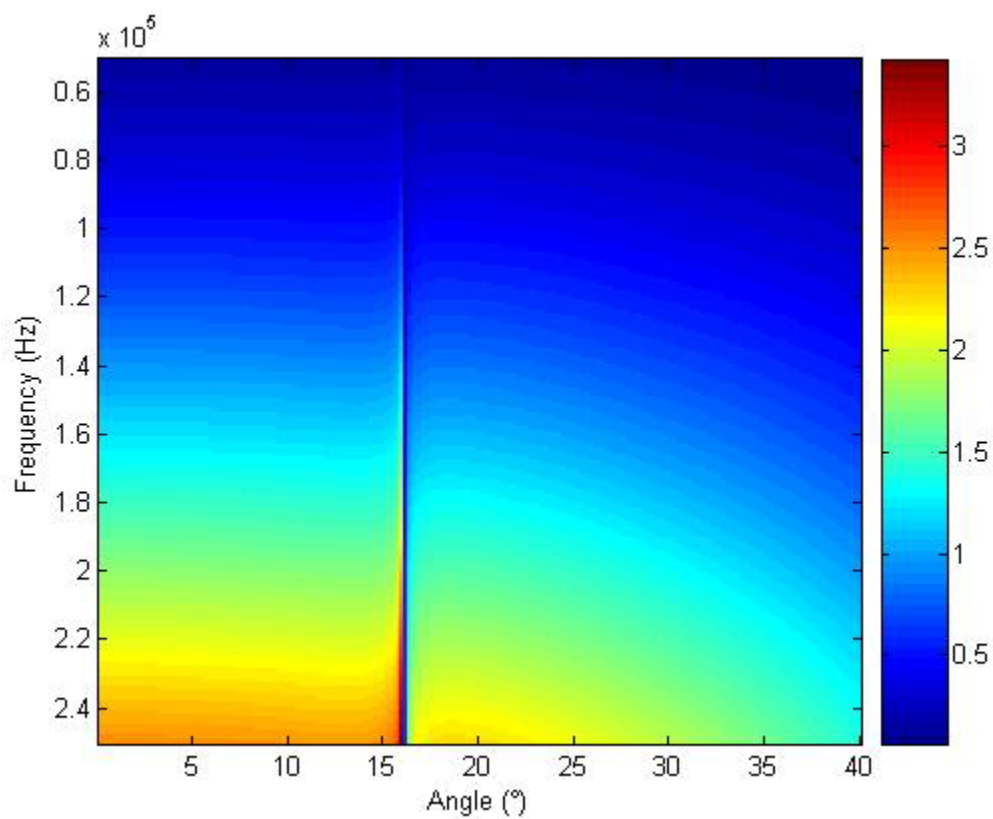


Figure 21. Contour plot of insertion loss (dB) prediction of ALUM-PR1574-ALUM 'sandwich' composite with properties as shown in Table 8.

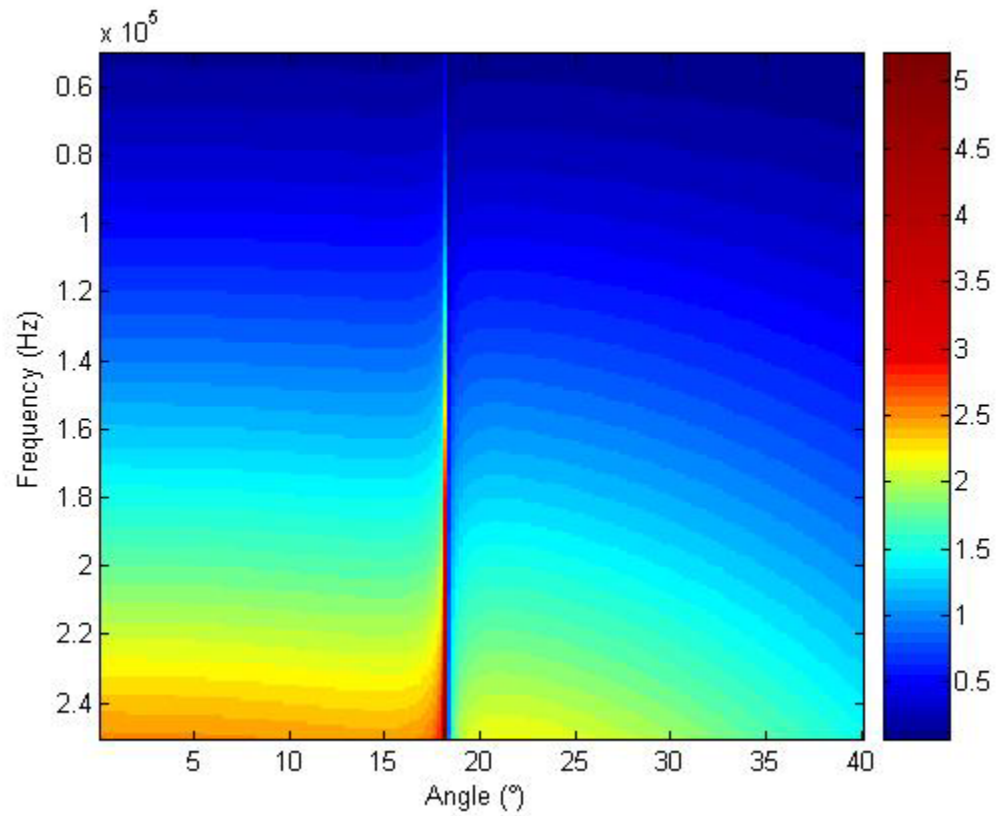


Figure 22. Contour plot of insertion loss (dB) prediction of ALUM-PR1574-ALUM 'sandwich' composite with properties as shown in Table 8, but with the Young's modulus of layers 1 & 3 changed to from 70 to 55GPa.

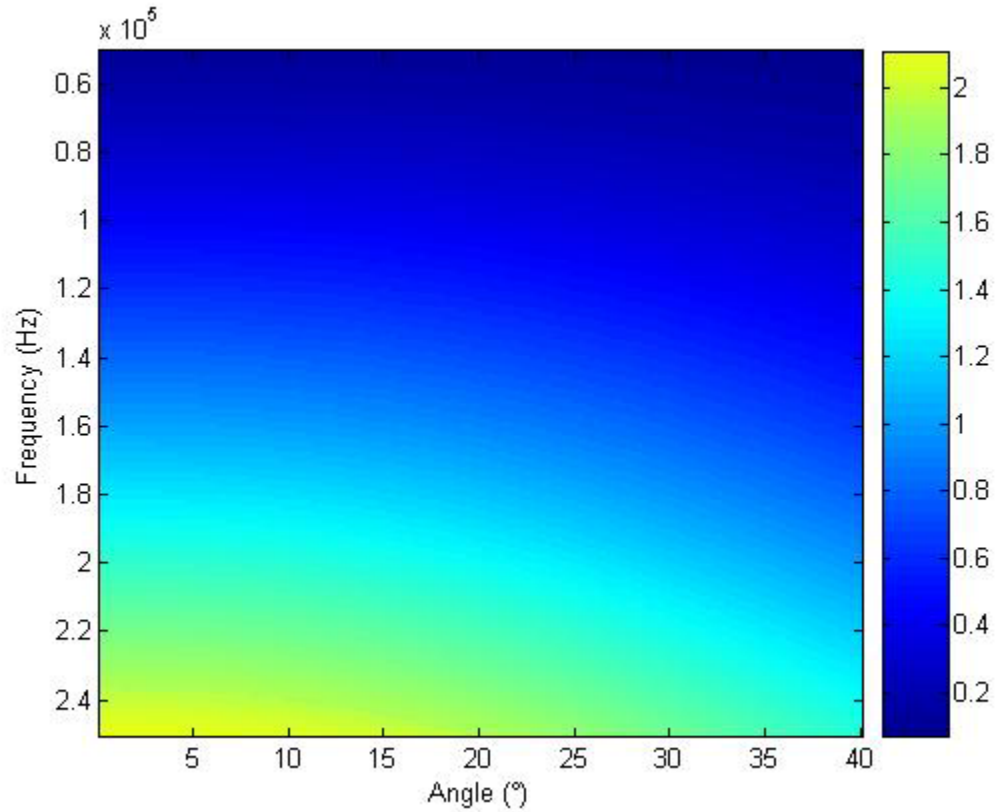


Figure 23. Contour plot of insertion loss (dB) prediction of ALUM-PR1574-ALUM 'sandwich' composite with properties as shown in Table 8, but with the Young's modulus of layers 1 & 3 changed to from 70 to 7GPa.

If the outer layer material is switched from Aluminum to A36 steel, with properties shown in Table 9, D increases by a factor of ~ 150 , relative to a single equivalent thickness layer of PR-1574. Insertion loss values, however, increase to unacceptable levels, as shown in Figure 24.

<i>Material</i>	<i>Density (g/cc)</i>	<i>Young's Modulus (GPa)</i>	<i>Tan δ</i>	<i>Layer Thickness (cm)</i>	<i>Poisson's Ratio</i>
Layer 1	7.7	207	0	.0635	0.29
Layer 2	1.03	0.20	.1	1.905	0.49
Layer 3	7.7	207	0	.0635	0.29

Table 9. Layered material 2: Steel-PR1574-Steel

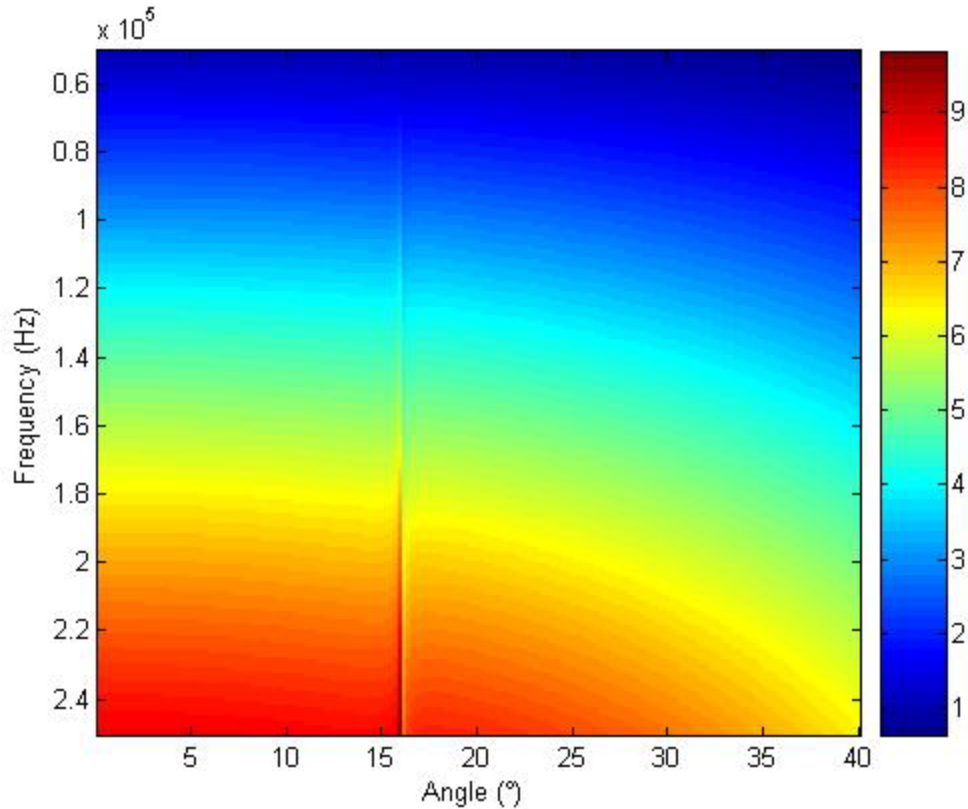


Figure 24. Contour plot of insertion loss (dB) prediction of STEEL-PR1574-STEEL 'sandwich' composite with properties as shown in Table 9.

These two examples demonstrate that a layered system can be designed to offer a structurally improved product, relative to the mono-layer design, with acceptable acoustic performance. In addition to improvement in bending rigidity, designs which use high strength outer layers offer improved performance relative to environmental loads as well. For example, a system of polyurethane sandwiched between metallic layers (i.e., steel, Alum) offers greatly reduced water absorption by the polyurethane, the ability to accept

off-the-shelf (OTS) surface treatments for fouling prevention, greater resistance to in-service wear/tear, greatly improved chemical resistance and reduced design restrictions in mounting schemes.

B. FUTURE WORK

The next logical step in this study is to improve the quality of model inputs for the layer design presented in Table 8 and to subsequently, upon acceptable model results, manufacture a layered panel according to that design and test for both acoustic and structural performance. This step results in model verification of a layered system after which the model can be used with confidence to optimize performance for application in specific cases.

It is important to note that the model does not consider the compatibility of layers with each other. Rather, it assumes perfect bonding between layers. For example, the case of PR-1574 and Aluminum is known to be a pair of materials that can be bonded together with little difficulty. This may not be the case for other combinations of high strength outer layers and polyurethane or rubber middle layers. Additionally, there likely exists a practical limit on minimum material thickness.

APPENDIX. MATLAB CODE

[illegible]

```

anglei(t)=angleinc.*t;
deg(t)=anglei(t)*57.3;%%%1 rad ~=57.3 degrees

for u=1:numfreqsteps;
    frequency(u)= 50000+(u.* 200000./(numfreqsteps));
    w= 2.*pi.*frequency(u);
    csw=1500;
    cswT=0 ;

    for n=1:numlayer

        Pscale(n)= v(n)./( (1+v(n)).*(1-(2*v(n)))));
        lambdai(n) = Pscale(n).*Ei(n); %%%%Lame's constant
        lambda(n)=real(lambdai(n));
        Pscale2(n)=(1./(1+v(n))).* ((v(n)/(1-(2.*v(n))))+ 1);
        SpeedtermLi(n)=Pscale2(n).*Ei(n);

        %%%%Calculate the tan d for the compressional wave %%%%
        LtanD(n)= imag(SpeedtermLi(n))/real(SpeedtermLi(n));
        %% The below terms are used in several locations %%%%
        TD = 1 + ((EtanD(n))^2);
        TD1=sqrt(TD);

        %%%% Calculate the effective Speedterm (modulus) for the
        %%%% compressional wave using the undamped modulus and
        %%%% the Young' loss tangent %%%%
        SpeedtermL(n)=2.*real(SpeedtermLi(n)).*(TD/(TD1+1));
        SpeedL(n)= sqrt((SpeedtermL(n))./rho(n));
        XciL(n)=sqrt( (rho(n)*(w^2)/(2*real(SpeedtermLi(n)))) * ((TD1-1)/TD) );

        %%%%Calculate the effective shear wave speed using the
        %%%%Young's modulus and poisson's ratio
        Pscale3(n)= 1./(2.*(1+v(n)));
        Gi(n)=Pscale3(n).*Ei(n);
        SpeedtermT(n) =(2*Gi(n))* (TD/(TD1+ 1));
        SpeedT(n)= sqrt(SpeedtermT(n)./rho(n));
        XciG(n)=XciL(n); %% Shear loss = Comp loss = Young's loss
        %% due to simplification made in Eq 17

        k(n)= (w./SpeedL(n));
        kappa(n)= (w./SpeedT(n));

        if n>1 %%%% If there is more than one layer %%%%
            angle(n)=asin (SpeedL(n).*Snell(n-1));
            Snell(n)=sin(angle(n))./SpeedL(n);
            angleT(n)= asin ( SpeedT(n).*Snell(n));
        else
            Snell1=(sin(anglei(t)))./csw;
            angle(n)=asin (SpeedL(n).*Snell1);
            Snell(n)=(sin(angle(n)))./SpeedL(n);
            angleT(n)= asin ( SpeedT(n).*Snell(n));
        end
    end
end

```

end

```
M(n)=(k(n).*sin(angle(n)))-(j*XciL(n));
Pa(n)=(k(n).*cos(angle(n)))-(j*XciL(n));
Qa(n)=(kappa(n).*cos(angleT(n)))-(j*XciG(n));
```

```
%%%%%%%%%%%%%%%%%%%%%%%%%%%%%%%%%%%%%%%%%%%%%%%%%%%%%%%%%%%%%%%%%%%%%%%%
%%%%%%%%%%%%%%%%%%%%%%%%%%%%%%%%%%%%%%%%%%%%%%%%%%%%%%%%%%%%%%%%%%%%%%%%
%%%%%%%%%%%%%%%%%%%%%%%%%%%%%%%%%%%%%%%%%%%%%%%%%%%%%%%%%%%%%%%%%%%%%%%% Matrix 1 = Potential state at z= thickness
%%%%%%%%%%%%%%%%%%%%%%%%%%%%%%%%%%%%%%%%%%%%%%%%%%%%%%%%%%%%%%%%%%%%%%%% NOTE: z is measured in the direction opposite to the incident
%%%%%%%%%%%%%%%%%%%%%%%%%%%%%%%%%%%%%%%%%%%%%%%%%%%%%%%%%%%%%%%%%%%%%%%% propagation
%%%%%%%%%%%%%%%%%%%%%%%%%%%%%%%%%%%%%%%%%%%%%%%%%%%%%%%%%%%%%%%%%%%%%%%%
%%%%%%%%%%%%%%%%%%%%%%%%%%%%%%%%%%%%%%%%%%%%%%%%%%%%%%%%%%%%%%%%%%%%%%%%
```

```
z=thk(n);
e1=exp((j*Pa(n)*z)-(XciL(n)*thk(n)));
e2=exp(-j*Pa(n)*z);
e3=exp((j*Qa(n)*z)-(XciL(n)*thk(n)));
e4=exp(-j*Qa(n)*z);
```

```
Kaya(n)=((((M(n)).^2)+((Pa(n)).^2)).*lambdai(n))+(2.*Gi(n).*((Pa(n)).^2));
```

```
A(1,1,n)=j*M(n).*e1;
A(1,2,n)=j*M(n).*e2;
A(1,3,n)=-j*Qa(n).*e3;
A(1,4,n)= j*Qa(n).*e4;
```

```
A(2,1,n)= j*Pa(n).* e1;
A(2,2,n)= -j*Pa(n).* e2;
A(2,3,n)= j* M(n).* e3;
A(2,4,n)= j* M(n).* e4;
```

```
A(3,1,n)=-j*Kaya(n).*e1;
A(3,2,n)=-j*Kaya(n).*e2;
A(3,3,n)=-j*2.*Gi(n).*M(n).*Qa(n).*e3;
A(3,4,n)=j*2.*Gi(n).*M(n).*Qa(n).*e4;
```

```
Q2=(Qa(n)).^2;
M2=(M(n)).^2;
A(4,1,n)=-j*2*Gi(n).*M(n).*Pa(n).*e1;
A(4,2,n)= j*2*Gi(n).*M(n).*Pa(n).*e2;
A(4,3,n)=-j*Gi(n).*(M2-Q2).*e3;
A(4,4,n)=-j*Gi(n).*(M2-Q2).*e4;
```

```
%%%%%%%%%%%%%%%%%%%%%%%%%%%%%%%%%%%%%%%%%%%%%%%%%%%%%%%%%%%%%%%%%%%%%%%%
%%%%%%%%%%%%%%%%%%%%%%%%%%%%%%%%%%%%%%%%%%%%%%%%%%%%%%%%%%%%%%%%%%%%%%%%
%%%%%%%%%%%%%%%%%%%%%%%%%%%%%%%%%%%%%%%%%%%%%%%%%%%%%%%%%%%%%%%%%%%%%%%% Matrix 2 = Potentials state at z=0 in the layer
%%%%%%%%%%%%%%%%%%%%%%%%%%%%%%%%%%%%%%%%%%%%%%%%%%%%%%%%%%%%%%%%%%%%%%%%
%%%%%%%%%%%%%%%%%%%%%%%%%%%%%%%%%%%%%%%%%%%%%%%%%%%%%%%%%%%%%%%%%%%%%%%%
```



```

z=0;
e1=exp((j*Pa(n)*z)-(XciL(n)*thk(n)));
e2=exp(-j*Pa(n)*z);
e3=exp((j*Qa(n)*z)-(XciL(n)*thk(n)));
e4=exp(-j*Qa(n)*z);

```

```

Kaya(n)=((((M(n)).^2)+((Pa(n)).^2)).*lambdai(n))+(2.*Gi(n).*((Pa(n)).^2));

```

```

A1(1,1,n)=j*M(n).*e1;
A1(1,2,n)=j*M(n).*e2;
A1(1,3,n)=-j*Qa(n).*e3;
A1(1,4,n)= j*Qa(n).*e4;

```

```

A1(2,1,n)= j*Pa(n).* e1;
A1(2,2,n)= -j*Pa(n).* e2;
A1(2,3,n)= j* M(n).* e3;
A1(2,4,n)= j* M(n).* e4;

```

```

A1(3,1,n)=-j*Kaya(n).*e1;
A1(3,2,n)=-j*Kaya(n).*e2;
A1(3,3,n)=-j*2.*Gi(n).*M(n).*Qa(n).*e3;
A1(3,4,n)=j*2.*Gi(n).*M(n).*Qa(n).*e4;

```

```

Q2=(Qa(n)).^2;
M2=(M(n)).^2;
A1(4,1,n)=-j*2*Gi(n).*M(n).*Pa(n).*e1;
A1(4,2,n)= j*2*Gi(n).*M(n).*Pa(n).*e2;
A1(4,3,n)=-j*Gi(n).*(M2-Q2).*e3;
A1(4,4,n)=-j*Gi(n).*(M2-Q2).*e4;

```

```

B(:, :, n) =A(:, :, n)*inv(A1(:, :, n));

```

```

if n>1
    Bi(:, :, n)=B(:, :, n-1)*B(:, :, n);
else
    Bi(:, :, n)=B(:, :, n);
end
end
B1=Bi;
B3=abs(B1);
Y1i=(((-1./B1(4,1)).*B1(4,2).*B1(2,1))+B1(2,2));
Y2i=(((-1./B1(4,1)).*B1(4,3).*B1(2,1))+B1(2,3));
Y3i=(((-1./B1(4,1)).*B1(4,2).*B1(3,1))+B1(3,2));
Y4i=(((-1./B1(4,1)).*B1(4,3).*B1(3,1))+B1(3,3));

```

```

Pn= (w/csw).*cos(anglei(t));%%%Pn in the first water layer
P1= (w/csw).*cos(asin (csw.*Snell(numlayer)));% P1 in last sw layer
Mn= (w/csw).*sin(anglei(t));%%%Mn in the first water layer
rhon=1000;

```

```

rho1=1000;
lambdan =rhon*(csw.^2);
Kayn=((Mn.^2)+ (Pn.^2)).*lambdan;

%%%Note: Kayn is Kay for the first of the two bounding water
%%%layers. G is zero in water so the expression is truncated
%%%compared to Kaya(n) used above. Lambda is found from the sound
%%%speed in water.
H3=(-Kayn*((-Y1i.*P1)+(Y2i.*rho1*(w^2)) ));
H4=( Pn*((-Y3i.*P1)+(Y4i.*rho1*(w^2))));

Trans1 =(-2.*rho1*Pn*Kayn);
Trans2 =rhon.*( (H3)+ (H4));

Trans = Trans1/Trans2;
TransIL(u,t)=(abs(Trans));
IL (u,t)=20*log10(1/TransIL(u,t));

end
end
%%%%%%%%%%%%%%%%%%%%%%%%%%%%%%%%%%%%%%%%%%%%%%%%%%%%%%%%%%%%%%%%%%%%%%%%END CALCULATIONS LOOP
%%%%%%%%%%%%%%%%%%%%%%%%%%%%%%%%%%%%%%%%%%%%%%%%%%%%%%%%%%%%%%%%%%%%%%%%

%%%%%%%%%%%%%%%%%%%%%%%%%%%%%%%%%%%%%%%%%%%%%%%%%%%%%%%%%%%%%%%%%%%%%%%% PLOTS %%%%%%%%%%%%%%%%%%%%%%%%%%%%%%%%%%%%%%%%%%%%%%%%%%%%%%%%%%%%%%%%%%%%%%%%%
subplot(1,3,1), plot(frequency,IL)
subplot(1,3,2), imagesc(deg,frequency,IL)
subplot(1,3,3), surf(deg,frequency,IL)

```

THIS PAGE INTENTIONALLY LEFT BLANK

LIST OF REFERENCES

1. L.J. Ziomek, Fundamentals of Acoustic Field Theory and Space-Time Signal Processing, Boca Raton: CRC, 1995.
2. L.E. Kinsler, A.R. Frey, A.B. Coppens, J.V. Sanders, Fundamentals of Acoustics 4th Edition, New York: John Wiley & Sons, not dated.
3. R.J. Bobber, Underwater Electroacoustic Measurements, Orlando: Naval Research Laboratory, July 1970.
4. G.B. Thurston and R. Stern, A Bibliography on Propagation of Sound through Plates, Willow Run Laboratories, Ann Arbor, MI, Report # 2784-1-S, 1959.
5. R.D. Fay, Notes on the Transmission of Sound through Plates, Journal of the Acoustical Society of America, V25, #2, 1953.
6. C.M. Thompson and R.Y. Ting, Journal of the Acoustical Society of America, V94, 1993.
7. C.L. Cartwright, Journal of the Acoustic Society of America, V112, Issue 5, 2005.
8. C.B. Officer, Introduction to the Theory of Sound Transmission, New York: McGraw-Hill, 1958.
9. L.M. Brekhovskikh, Waves In Layered Media, London: Academic Press, 1960.
10. L.E. Malvern, Introduction to the Mechanics of a Continuous Medium, Englewood Cliffs: Prentice Hall, Inc., 1969.
11. J.F. Nye, Physical Properties of Crystals, Oxford: Clarendon Press, 1985.
12. R.N. Capps, Elastomeric Materials for Acoustical Applications, Orlando: Naval Research Laboratory, September 1989.
13. H.T. Loeser, Sonar Engineering Handbook, Los Altos: Peninsula Publishing, 1982.
14. G.J. Roche, "Investigation of Candidate Materials for Upsounder/Downsounder Acoustic Window Applications," Naval Undersea Warfare Center, Newport, RI, Tech Mem-990103, 1999.
15. R.M. Jones, Mechanics of Composite Materials, New York: McGraw-Hill, 1975.
16. E. Reissner, Journal of Applied Mechanics V12, 1945.

THIS PAGE INTENTIONALLY LEFT BLANK

INITIAL DISTRIBUTION LIST

1. Defense Technical Information Center
Ft. Belvoir, Virginia
2. Dudley Knox Library
Naval Postgraduate School
Monterey, California
3. Technical Library
Naval Undersea Warfare Center-Division Newport
Newport, Rhode Island
4. Ken Webman
Naval Undersea Warfare Center-Division Newport
Newport, Rhode Island
5. Kevin Smith
Naval Postgraduate School
Monterey, California
6. Clyde Scandrett
Naval Postgraduate School
Monterey, California
7. Thomas Ramotowski
Naval Undersea Warfare Center-Division Newport
Newport, Rhode Island
8. Tony Paolero
Naval Undersea Warfare Center-Division Newport
Newport, Rhode Island